3.09 Nanoscale Mineral Decay and Its Importance in Geomorphology

Ronald I. Dorn[a], Steven J. Gordon[b], and Ara Jeong[c], [a] School of Geographical Sciences and Urban Planning, Arizona State University, Tempe, AZ, United States; [b] Department of Economics and Geosciences, United States Air Force Academy, Colorado Springs, CO, United States; and [c] Research Institute of Future Land, Korea University, Seoul, Republic of Korea

3.09.1	**Introduction to nanoscale mineral and rock decay**	**117**
3.09.2	**Nanoscale techniques and interpretation issues in geomorphology**	**118**
3.09.2.1	Nanoscale resolution microscopy	118
3.09.2.2	Linking scales through digital image processing	120
3.09.2.3	Crossing the nanoscale to micron-scale threshold	121
3.09.3	**Applying nanoscale strategies to rock decay forms**	**123**
3.09.3.1	Case hardening	123
3.09.3.2	Tafoni	124
3.09.3.3	Arctic & alpine settings	124
3.09.3.4	Splintering and nanoscale etching	125
3.09.4	**Nanoscale processes as a limiting factor in erosion**	**127**
3.09.4.1	G.K. Gilbert's weathering-limited landscapes	127
3.09.4.2	Detachment-limited pediment & strath erosion	130
3.09.5	**Nanoscale biological mineral decay**	**130**
3.09.5.1	Ants as agents of carbon dioxide sequestration	130
3.09.5.2	Biological processes and the fallacy of Goldich's weathering sequence	134
3.09.6	**Nanoscale processes and dust generation**	**138**
3.09.7	**From nanoscale to landscape scale: Applications of meteoric ^{10}Be and ^{10}Be/^{9}Be to the study of Earth's surface**	**142**
3.09.8	**Conclusion**	**143**
Acknowledgments		**145**
References		**145**

Glossary

Authigenic phase The phase resulting from the adsorption of previously dissolved elements in the water column overlying the sampled sediments.

Back-scattered electron (BSE) microscopy An accelerated electron beam in an electron microscope produces collisions between electrons and atoms, where the largest atoms with the higher atomic number (Z) generate a "brighter" intensity when imaged with a back-scattered detector.

Biotic weathering Mineral weathering caused by life, including bacteria, fungi, algae, plants, and animals.

Case hardening The outer shell of a rock that has been hardened (indurated) through the addition of elements such as silica or iron.

Cosmogenic nuclides Rare nuclides produced by high-energy cosmic ray induced nuclear reactions in the atmosphere (meteoric) or in surface rocks and minerals (*in situ*-produced). There are stable (e.g., ^{3}He) and radioactive (e.g., ^{14}C, ^{10}Be, ^{26}Al, ^{36}Cl) cosmogenic nuclides and used for a variety of applications in geomorphology.

Etching of minerals Mineral dissolution is not an even produce; areas of more intense dissolution are seen as pits on the scale of micrometers.

Heavy metal scavenging Iron and manganese oxides and hydroxides scavenge heavy metals such as zinc, copper, and lead.

High resolution transmission electron microscopy (HRTEM) 2-D spatial imaging if very thing samples able to image mineral lattices with a spatial resolution of greater than 0.08 nm.

Meteoric ^{10}Be ^{10}Be produced in the Earth's atmosphere (half-life: 1.39 Ma) that is often utilized as process tracers in Earth's environment.

Microfractures Breaks in minerals that can carry capillary water.

Nanoscale Features between one nanometer (10^{-9} m) and 100 nm (10^{-7} m) or 0.1 μm.

Treatise on Geomorphology, Second Edition, 2022, 116–150

Splintering Rock fracturing in a pattern of subparallel fractures that resembles a book that has been thrown in water and then dried.

Thermal fracturing Breaking of minerals from the process of heating and cooling, such as the passage of a wildfire over rock surfaces.

3.09.1 Introduction to nanoscale mineral and rock decay

Scale is a vitally important concern in the development of geomorphic weathering theory (Finlay et al., 2020Hall, 2006a, 2006b; Matsuoka et al., 2017a, 2017b; Phillips, 2000; Pope, 2015; Turkington et al., 2005; Viles, 2001). Scale is a key variable in the boundary layer model designed to interpret spatial variability in weathering (Pope et al., 1995). Scale have consumed much thought and research trying to link the largely disparate weathering subfields of controlled laboratory studies and field-based investigations (Banfield and Barker, 1994; Brantley, 2005; Brantley and Mellott, 2000; Brantley and Velbel, 1993; Casey et al., 1993; Hellmann et al., 2012; Matsuoka et al., 2017b; Meunier et al., 2007; Navarre-Sitchler and Brantley, 2007; Nishiyama and Yokoyama, 2017; Putnis and Ruiz-Agudo, 2013; Swoboda-Colberg and Drever, 1993; Turkington and Paradise, 2005; White, 2005; Yokoyama and Nishiyama, 2017; Zhu et al., 2006).

Thresholds are also an important focus in geomorphic weathering research (Paradise, 1995; Pope et al., 2002). A key scale threshold exists between nanoscale processes and those operating even at the micron-scale. In his 2001 presidential address to the Geochemical Society, Michael Hocehlla, Jr. emphasized: "nanoscience is based on the premise that materials properties in the bulk do not simply scale into the nanodomain, but property modification, and in some cases entirely different properties, are to be expected … In the nanoscale size range, physical, electrical, magnetic, thermal, kinetic, and other properties can be altered dramatically simply due to the physical dimensions of the material" (Hochella, 2002a, 2002b, p. 738).

Interactions at the micron-scale simply do not reflect molecular dynamics in the nanoscale chemical environment, in part because processes at the nanoscale can undergo substantial changes when exposed to water (Hovelmann et al., 2018; Kalinichev et al., 2007; Putnis, 2019; Wang et al., 2006; Zhang et al., 2003). Putnis and Ruiz-Agudo (2013: 177) explain the basics:

> When minerals come into contact with aqueous fluids with which they are out of equilibrium, reactions begin as the new system seeks to establish a new equilibrium (lower energy state). If the aqueous fluid is undersaturated with respect to a mineral, the mineral will dissolve until the fluid becomes saturated with the mineral phase. However, if the fluid becomes supersaturated with any new mineral phase, the latter may precipitate by nucleation and subsequently grow.

Nanoscale is typically defined as examining features between one nanometer (10^{-9} m) and 100 nm (10^{-7} m) or 0.1 microns (Fig. 1). One way to visualize the nanoscale is to look at your hand; the scale jump between the entire Earth and your hand is the same dimensional scale difference as the jump from your hand to a nanoparticle. Nanoscale processes are not included in the "microscale," defined by Pope et al. (1995: 220) as being submillimeter, because a very different realm of weathering processes operate below 0.1 μm. Research on nanoscale weathering is no longer in its infancy, having grown up with progressive improvements in high resolution transmission electron microscopy (HRTEM) since the 1980s. The first of this research tended to focus on the very different water-mineral interaction that occurs in the nanodomain within minerals, in that even microfracture capillary water (Meunier et al., 2007) behaves differently from water held within mineral internal surfaces (Hochella, 2002b). The first two decades in the 21st century has seen a diversification of nanoscale weathering research (Matsuoka et al., 2017a; Mantha et al., 2019; Putnis, 2019), including the beginnings of attention paid to connections between geomorphology and nanoscale processes (Basile-Doelsch et al., 2015; Finlay et al., 2020; Lybrand et al., 2019; Yokoyama and Nishiyama, 2017).

After introducing nanoscale techniques and issues related to geomorphic interpretation, this article covers case studies in four different areas: interpreting forms of rock decay; nanoscale processes limiting rates of erosion; biological mineral decay at the nanoscale; the importance of nanoscale processes related to dust generation, and some applications of meteoric ^{10}Be. Exactly how the study of nanoscale rock and mineral decay will alter the field of geomorphology is severely limited by the relatively few number of geomorphologists who study these processes. Not enough researchers have carried out at the nanoscale to reach a critical mass of scientists to discuss cohesive theory-building on connections with landform evolution. That is why this review consists of a series of case studies organized around geomorphic themes. Thus, our hope is that a dialogue will develop on how the nanoscale connects to broader theoretical issues in geomorphology. Such an informed dialogue, however, will require that more geomorphologists engage in nanoscale geomorphic research.

Please note that we try to eschew here, as much as possible, the term "weathering" for the reasons explained by Hall et al. (2012) and also in the Dixon and Hall article of this volume. We will use instead the suggested term rock decay. Sometimes, however, the term weathering is simply too ensconced at the present time to completely discard and we feel forced to use weathering in certain contexts.

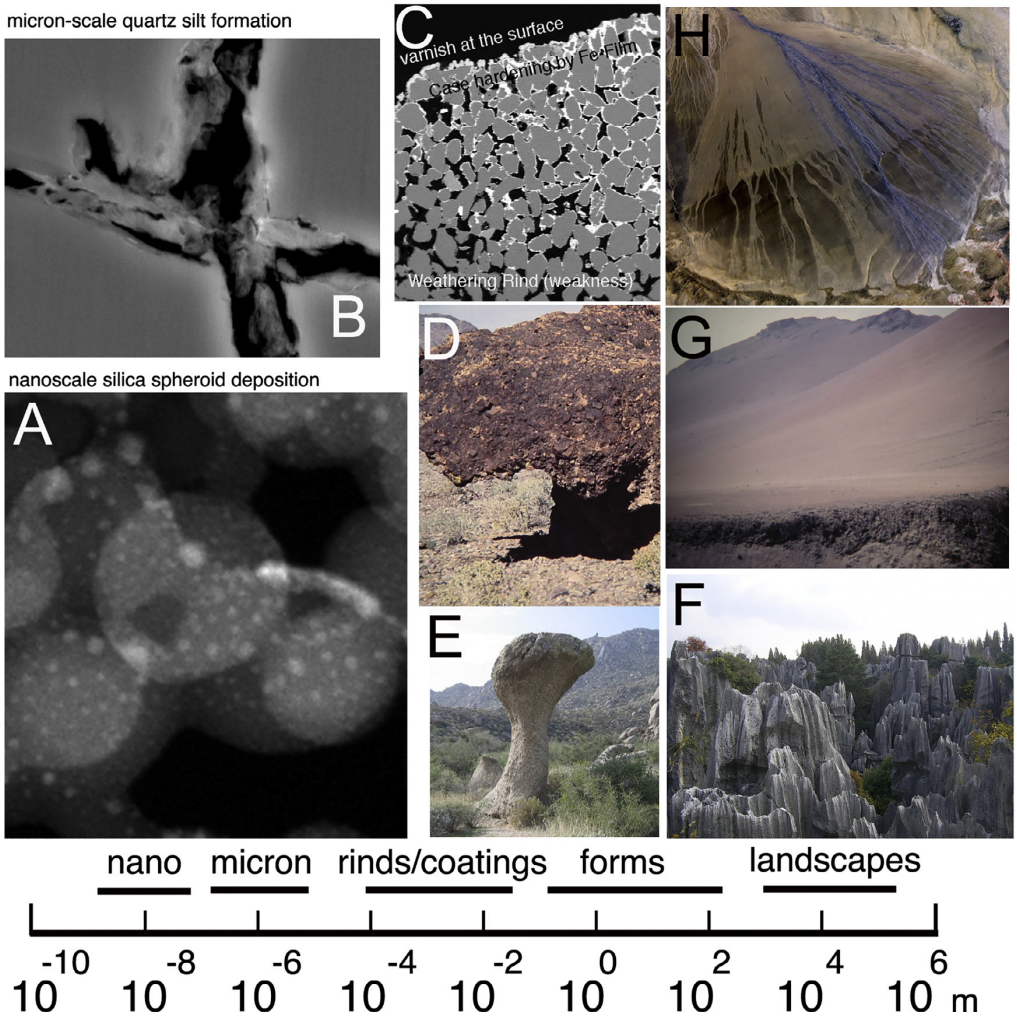

Fig. 1 Visualization of nanoscale weathering placed within broader spatial scales of weathering phenomenon. Examples presented from nano to landscape scales are: (A) nanoscale silica spheroids a few tens of nm across from silica glaze in Tibet (HRTEM image); (B) micron-scale silt formation from quartz weathering in Arizona (BSE image); (C) millimeter to centimeter-scale rock coatings and weathering rinds illustrated from Wyoming (BSE image) and (D) Death Valley (case hardened rock shelter); (E) meter-scale weathering forms of a "mushroom rock", Arizona and (F) limestone karst stone forest, Kunming; and (G) kilometer-scale weathering landscapes of a salt-encrusted marine terrace, Peru and (H) varnish-coated alluvial fan, western China. The alluvial fan Aster alluvial-fan image is courtesy of NASA; other images are from the authors.

3.09.2 Nanoscale techniques and interpretation issues in geomorphology

3.09.2.1 Nanoscale resolution microscopy

The study of earth materials has been enhanced in the past two decades through the use of high-resolution transmission electron microscopy (HRTEM) and other precision techniques. Ongoing technique developments over the past four decades has led to an array of imaging and analysis tools available to examine weathering processes and products (**Table 1**). Each technique has its advantages and limitations that are reviewed in detail elsewhere (Lee, 2010) with a useful review on strategies to understand bacteria and fungal interactions by Balogh-Brunstad et al. (2020). Mitchell et al. (2021) also offer a useful strategy of bringing many of the methods in **Table 1** together called "correlative microscopy" that crosses dimensions (2D-3D) and scales (from nm to cm). This section overviews a few methods that we have used here or could be used in geomorphological studies of nanoscale mineral and rock decay.

The basic idea behind most high-resolution microscopy is to thin a sample enough so that electrons can pass through the sample upon irradiation with a 80–300 kV electron beam. Given the nature of the material and the particular techniques

Table 1 Overview of nanoscale microscopy techniques useful in rock decay research.

Technique (and acronym)	*Information obtained*	*Spatial resolution*	*Limitations*
Coupled dual-beam focused ion beam electron microscopy (FIB-EM)	Used to create and image cross-sections *in situ*, widely used to extract sections for TEM analysis. Real time imaging in SEM mode during ion milling	>∼1 nm	Maximum sample and scan size, requires vacuum, Ga ion implantation
High resolution transmission electron microscopy (HRTEM)	2-D spatial imaging, lattice imaging	>0.08 nm	Small area, sample preparation challenges, sample thickness <50 nm
Energy dispersive X-ray analysis (EDX)	Elemental composition, X-ray mapping of elements	>1 nm (HRTEM); >20 nm (SEM)	Detection limit varies, ∼0.2 Wt.%. Difficult for light element detection
Energy-filtered TEM (EFTEM)	Mapping of elements detectable from EELS spectrum	<1 nm	Best results with light elements, requires high vacuum and thin specimens
Scanning Transmission Electron Microscopy (STEM)	2-D special imaging, high contrast	<1 nm	Requires vacuum, thin specimen
Scanning electron microscopy (SEM) with back-scattered electron detector (BSE)	Average atomic number (Z) revealed through contrast I grayscale image	>5 nm	Generally requires vacuum (dry samples), sample size dependent on chamber size
Scanning electron microscopy (SEM) with secondary electrons (SE)	2-D spatial imaging	>1 nm	Requires vacuum, sample size dependent on chamber size
Atomic Force Microscopy (AFM or FM)	3-D surface microtopography	<1 nm in Z, <10 nm X,Y	Maximum scanning area of about 150 × 150 μm. Flat samples ideal
Secondary ion mass spectroscopy (SIMS)	Elemental and isotopic composition	50 nm with NanoSIMS	Requires vacuum, damages analysis region

used the thickness for high-resolution imaging can vary from ∼10 to 50 nm. Today most high-resolution TEM specimens are prepared using a coupled dual-beam focused ion beam electron microscopy (FIB-EM). The FIB-EM can site specifically ion mill and deposit metals; coupled with a micromanipulator the FIB-EM can extract features/regions on the order of 10–30 μm wide and carry out nanoscale tomography (Schiffbauer and Xiao, 2009). Once extracted and mounted to a TEM grid *in situ* the FIB-EM is used to thin the extracted region until it becomes electron transparent and usable in the TEM (often referred to as a lamella) (Brown and Lee, 2007). FIB-EM prepared samples have many advantages, such as allowing investigators to see the context of a lamella in BSE, SE, STEM, and EDX modes prior to breaking vacuum and moving the specimen to a TEM for higher resolution analysis. Other techniques used to prepare samples for TEM include mechanical crushing of minerals, which can generate edges that are sufficiently electron transparent and ultramicrotoming, which can prepare electron transparent slices of material using a diamond knife. Tripod polishing and precision ion polishing (PIPS) are also useful for obtaining electron transparent areas from bulk specimens for TEM analysis.

The reader who has not yet utilized modern scanning/transmission electron microscopes (TEM/STEM) should be aware of the need for understanding careful sample preparation and technical details. For example, imaging starts with placement of the TEM grid into a sample holder and insertion of the holder through an airlock, into a high vacuum electron column. HRTEMs use much higher electron beam voltages (typically from 80 to 300 kV) than SEMs used by a lot of weathering researchers. The high voltage, coupled with a thin sample, decreases interaction volume and allows EDX measurements to be made with spot sizes of <10 nm, in contrast to typical SEM interaction volumes on the order of ∼1 μm at 15 kV with thicker/bulk samples. Higher voltage has disadvantages that can become advantages; for example, we illustrate how beam damage on thin samples, leaving behind a series of holes or grid patterns (e.g., Lee, 2010: 10) can be used in nanoscale mapping of mineral decay. In general, the high spatial resolution of STEM and the ability to utilize atomic number (Z) contrast makes it a particularly powerful tool in weathering studies (Brown and Lee, 2007).

Nanoscale studies generate a variety of different types of imagery, formed by filtering scattered electrons. Bright-field images are generated from a direct beam that contains unscattered and low-angle forward scattered electrons. Dark-field images, in contrast, are generated only from forward-scattered electrons. The thickness, atomic number and Bragg diffraction (in crystalline material) will control the angle of scattering and the intensity of scattering—all creating the HRTEM image. Since mineralogy is often important in weathering, electron diffraction patterns record the angular distribution of electrons where minerals can be identified by the spacing of spots using selected-area electron diffraction (SED), precession electron diffraction (PED), or convergent-beam electron diffraction (CBED). It is also possible to generate images of specific elements at the subnanoscale using energy-filtered TEM imaging that takes a specific region of an EELS spectrum to form an image.

Compositional analysis is typically carried out by energy dispersive X-ray spectroscopy (EDX) for higher atomic number elements, and electron energy loss spectroscopy (EELS) for lighter elements. EELS measures energy lost through ionization of sample atoms, separating electrons according to the energy they have lost. EELS can measure elemental abundance and also determine valence states at spatial resolutions less than one nanometer.

3.09.2.2 Linking scales through digital image processing

An increasingly important weathering literature focuses on explaining offsets between field-based quantification of weathering and laboratory studies of weathering rates (Banfield and Barker, 1994; Brantley, 2005; Brantley and Mellott, 2000; Brantley and Velbel, 1993; Casey et al., 1993; Hellmann et al., 2012; Matsuoka et al., 2017b; Meunier et al., 2007; Navarre-Sitchler and Brantley, 2007; Nishiyama and Yokoyama, 2017; Putnis and Ruiz-Agudo, 2013; Swoboda-Colberg and Drever, 1993; Turkington and Paradise, 2005; White, 2005; Yokoyama and Nishiyama, 2017; Zhu et al., 2006). Brantley (2005, p. 108) concisely summarized some key issues:

> … extrapolating from one scale to another (scaling up) is often not quantitatively successful. For example, quantitative extrapolation of laboratory rates to field systems remains difficult, and we now recognize that multiple factors contribute to this discrepancy… Of particular importance is the reactive surface area of dissolving minerals: this term must be investigated and understood more thoroughly. In addition, laboratory rates are generally measured far from equilibrium, whereas natural weathering often occurs closer to equilibrium where dissolution is slower… The scaling-up problem inherent in the laboratory-field discrepancy may well be solved through increased understanding developed as we bridge scales of analysis from the nano to global scale…

Meunier et al. (2007: 432) explicitly advocates that the missing link in bridging scales rests at the scale of hand specimens:

> As weathering is a multi-scale phenomenon, theoretically any model needs to integrate the solid-fluid exchanges from the atomic interactions at the very surface of primary and secondary minerals (nanometer), to the rock sample (decimeter) and finally to the watershed (kilometer)… The extensive use of high-resolution transmission electron microscopy (HRTEM), atomic force microscopy (AFM) and spectroscopy have significantly improved our knowledge of fluid-mineral reactions and their related interactions. Conversely, the large-scale studies based on isotope mass balance methods provide denudation rates for provinces or continents. Surprisingly, it is at the hand-specimen scale where efforts should now be directed.

One strategy that could help bridge the discrepancy at the hand sample level is *in situ* quantitative analysis of mineral dissolution (Dorn, 1995) using digital image processing (e.g., **Fig. 2**). This direct measurement of mineral dissolution has led to an understanding of field relationships on the temperature dependence of weathering (Dorn and Brady, 1995), and understanding of the effects of rainfall and temperature on mineral weathering (Brady et al., 1999), long-term rates of glass dissolution (Gordon and Brady, 2002), and the role of lichens and rock coatings on field mineral weathering rates (Gordon and Dorn, 2005a, 2005b).

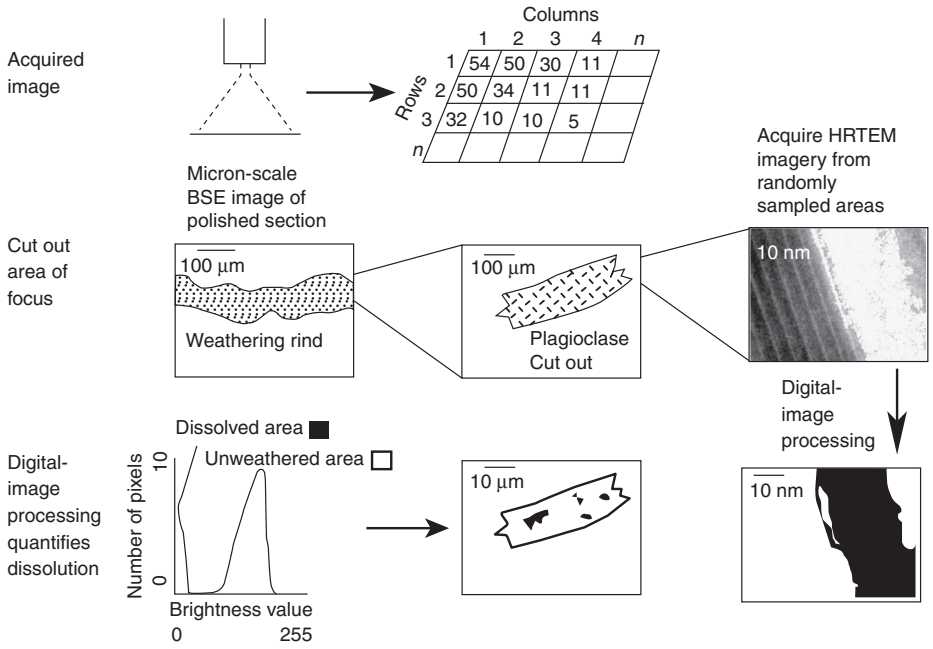

Fig. 2 Connecting field and lab results, as well as rescaling weathering rates is feasible using digital image processing of dissolved minerals. Originally developed for measuring weathering rates over thousands of years in field samples at the micron scale with BSE imagery, this approach can also directly compare laboratory with field samples and the same samples at scales ranging from square nanometers to square millimeters.

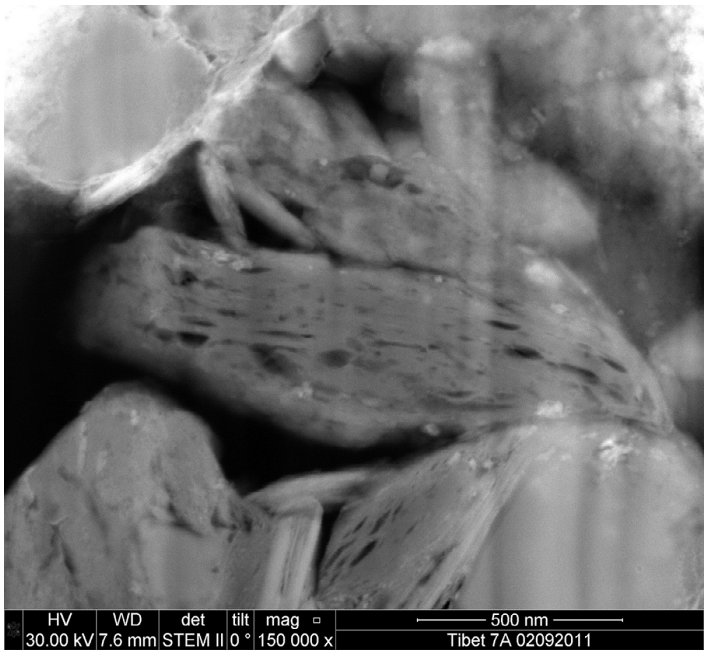

Fig. 3 High resolution BSE images are ideal for measuring mineral dissolution, where black areas are dissolution voids as seen in this image of dust particles resting on a sample from the Akesu Volcanic field, Tibet. Prior to digital image processing, each mineral would be "cut out" separately and made into its own image. Then, the void spaces would be made its own image and counted digitally given an area of the mineral that has dissolved (cf. Dorn, 1995).

Although digital image processing of BSE imagery has only been used to analyze field weathering that has taken place over 10^1 to 10^5 years and at the micron scale, there is no reason why laboratory samples or nanoscale samples could not be similarly analyzed. For example, the subnanometer conduits that carry aqueous fluids (Banfield and Barker, 1994) or the nanoscale etch pits could be prepared for digital image processing to quantify nanoscale porosity (**Fig. 2**).

Previous research on digital image processing to quantify weathering focused on the micron scale, typically measuring 10^5 square microns of mineral cross sections imaged with BSE per field site. New advances in electron microscopy increased the resolution of back-scatter images. It is now possible to analyze mineral dissolution at the nanoscale with BSE (e.g., **Fig. 3**). "Scaling-up" (cf. Brantley, 2005: 108) and then "scaling-down" becomes a task of taking lower resolution BSE and higher resolution BSE images using STEM at different scales and measuring *in situ* dissolution. Measurement of field and laboratory weathered samples alike at different scales, thus, enables the integration of data to the hand sample level—as advocated by Meunier et al. (2007).

3.09.2.3 Crossing the nanoscale to micron-scale threshold

There is a danger involved in extrapolating nanoscale weathering observations to smaller scales (larger areas). Misunderstanding of the threshold between processes operating at the micron-to-meterscale versus the nanoscale environment can lead to confusion and misinterpretation. An example comes from the rock varnish literature where nanoscale instability was simply assumed to invalidate (Garvie et al., 2008, 2009) observations at the micron scale of over 10,000 microlamination sequences (e.g., **Fig. 4**) recording paleoclimatic fluctuations (Liu, 2003, 2010; Liu and Broecker, 2000, 2007, 2008a, 2008b; Liu et al., 2000; Zhou et al., 2000). In summary, Garvie et al. (2008, 2009) analyzed only three samples with HRTEM at the nanoscale, finding evidence for nanoscale instability of manganese oxides. Garvie et al. (2008, 2009) made the mistake of simply assuming that nanoscale instability meant that micron-scale paleoclimatic interpretations of over a decade rock varnish research by T. Liu and colleagues must be invalid. That is an invalid assumption.

The issue here is not a problem with the basic observation of nanoscale instability. Prior to Garvie et al. (2008, 2009), others noted that nanoscale instability of Mn-oxides is the key to explaining how rock varnish forms (Dorn, 1998, 2007; Krinsley, 1998; McKeown and Post, 2001; Potter, 1979). In the polygenetic model of varnish formation, micron-scale microbial processes fix Mn and Fe oxides (**Fig. 5**), followed by nanoscale instability that moves Mn and Fe oxides between bacterial casts and clay minerals. Ongoing shuffling of Mn-Fe oxides reoccurs at the nanoscale to cement clays and Mn-Fe oxides to rock surfaces and to previous layers of varnish (Dorn, 2007; Krinsley, 1998; Krinsley et al., 2017).

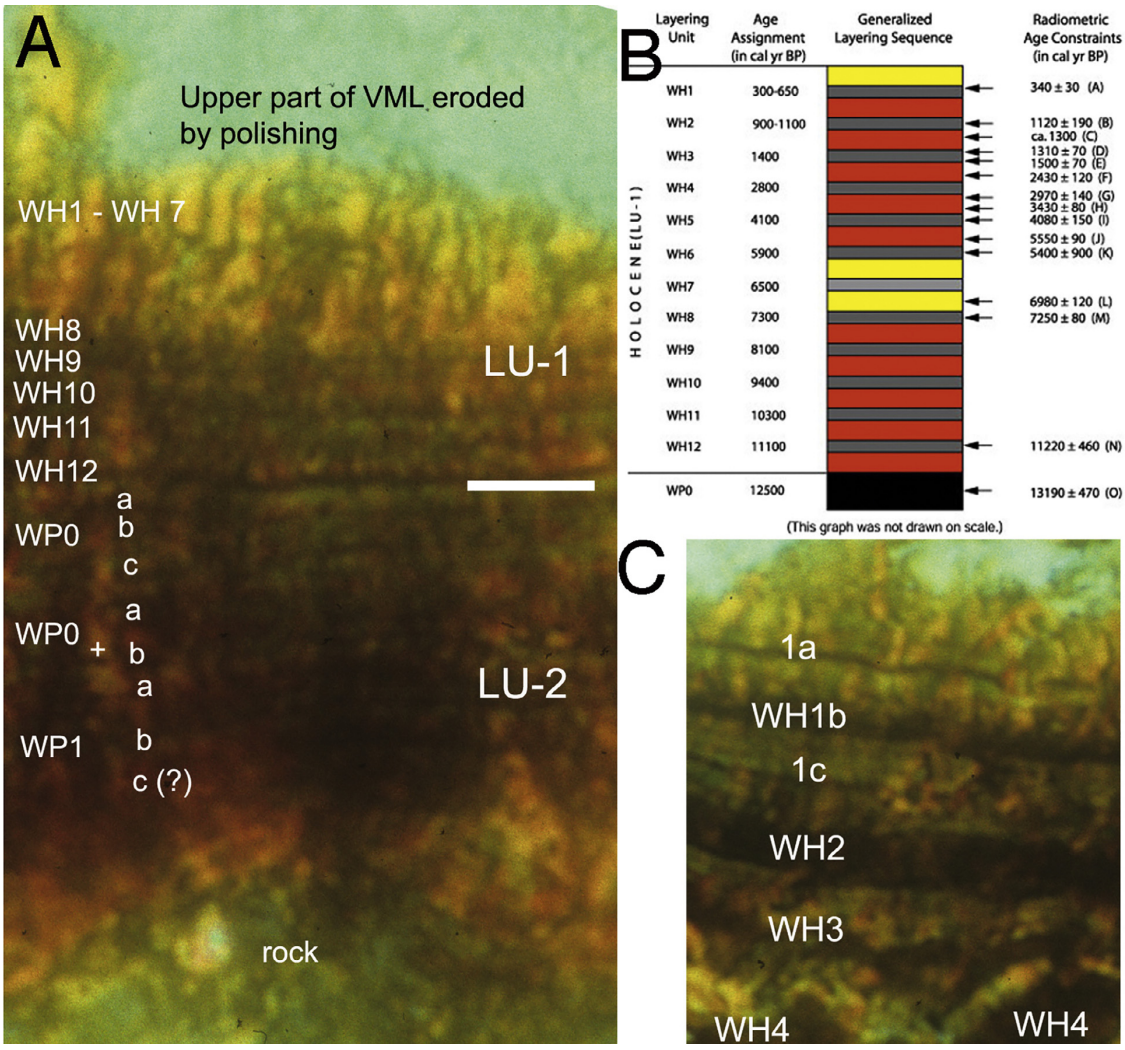

Fig. 4 Microsedimentary basins with high rates of varnish accumulation show varnish microlaminations recording Holocene climatic changes. Black bands formed during wet periods in the Holocene termed WH (for wet Holocene), and multiple black bands in the terminal Pleistocene black layers WPO (Younger Dryas, wet Pleistocene black layer zero) and WP1 (wet Pleistocene black layer 1). Under the right conditions of fast accumulating varnish and proper thin section procedures, millennial and submillenial wet periods can be used successfully in geomorphic research (Liu and Broecker, 2008a). These climatic signals are seen here in an example from debris flows at South Mountain, Arizona, where the varnish microlamination method successfully predicted that debris flows would occur (Dorn, 2016), despite prior thinking that no such hazard existed in the Sonoran Desert (Péwé, 1978).

While nanoscale instability is a key to varnish formation, it does not invalidate micron-scale processes—as Garvie et al. (2008, 2009) naively assumed. As Krinsley (1998, p. 721) explained: "at the spatial scale of microns… some varnish appears quite stable with distinct layering patterns… At the spatial scale of nanometers as viewed with HRTEM, varnish appears to be in an open system… This is analogous to automobiles moving in a crowded parking lot, with oxides moving around until they find a suitable parking space in clay minerals." Cars moving in a parking lot does not imply that the parking lot itself is unstable.

The broader issue here is that the geochemistry newly formed mineral material at the nanoscale involves a great number of unknown issues. Every investigator who has explored, for example, varnish at the nanoscale agrees that Mn and Fe oxide instability is common (Dorn, 1998, 2007; Krinsley, 1998; Krinsley et al., 1990, 1995, 2017; Macholdt et al., 2015; McKeown and Post, 2001; Garvie et al., 2008, 2009), but HRTEM nanoscale observations do nothing to invalidate the extensively replicated-scale stratigraphy (Liu, 2003, 2010; Liu and Broecker, 2000, 2007, 2008a, 2008b; Liu et al., 2000; Zhou et al., 2000). This example highlights just one of the dangers of extrapolating nanoscale observations to even micron-scale phenomena.

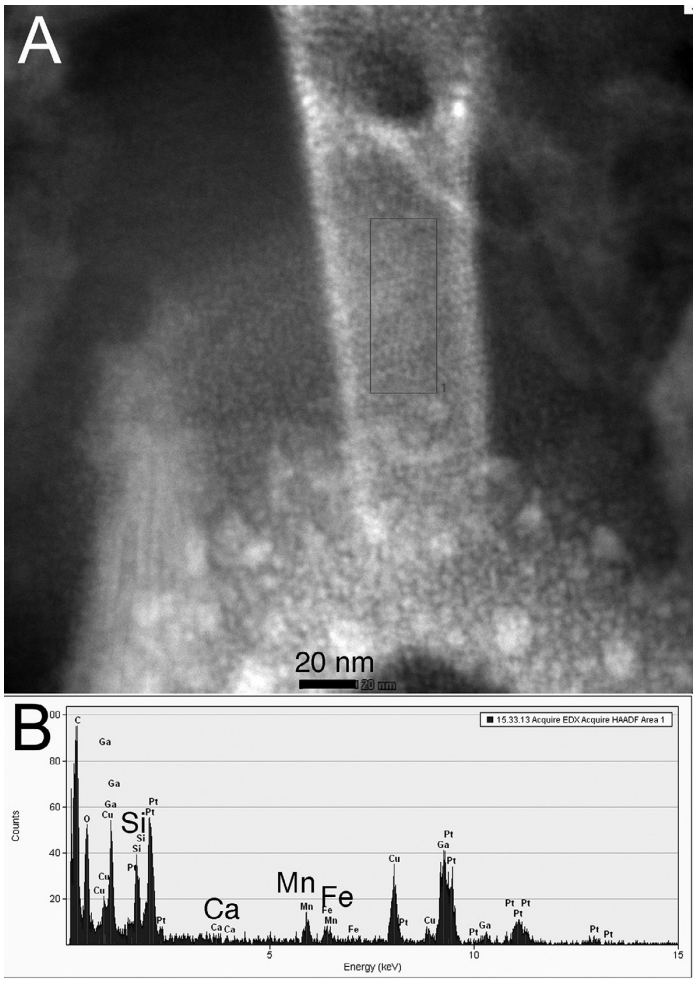

Fig. 5 Nanoscale instability of manganese and iron is key to the formation of rock varnish. (A) Budding bacteria hyphae form (Krinsley et al., 2017) emerging from a cocci-form. The EDS spectra measured in the box consists mostly of artifacts associated with mounting and preparation of the sample. However, annotation of the EDS spectra with a larger font identifies the composition of the hyphae form as mostly Mn and Fe, with some Si and Ca. Notice that the granules of Mn-Fe mobilize from bacterial sheath fragments, are transported a few nanometers, and then are fixed into mixed-layered illite-montmorillonite clays. These nanometer-scale Mn-oxides can be remobilized and refixed over and over again in a shifting nanoscale mineral structure (McKeown and Post, 2001: 712). However, this nanoscale remobilization does not erase the varnish lamination layers observed at the micron scale (**Fig. 4**).

3.09.3 Applying nanoscale strategies to rock decay forms

This section presents different areas of research in geomorphology where attention to the nanoscale has either yielded or has the potential to yield new insights.

3.09.3.1 Case hardening

Case hardening of the outermost shell of a rock involves the migration of rock coating constituents into pore spaces in the weathering rind of minerals (**Fig. 6**A) and the outer rim of a rock (Conca and Rossman, 1982; Dorn, 2009; Dorn et al., 2012, 2017; Gordon and Dorn, 2005a). At first, it might seem counterintuitive to think that both dissolution and precipitation of new mineral matter can occur together, but both processes do operate in tandem at the nanoscale (e.g., Emmanuel, 2014). The dissolution of a variety of different rock coatings that have formed on top of a weathering rind produces case hardening; this section focuses on two of the most common remobilized rock coatings: silica glaze and rock varnish.

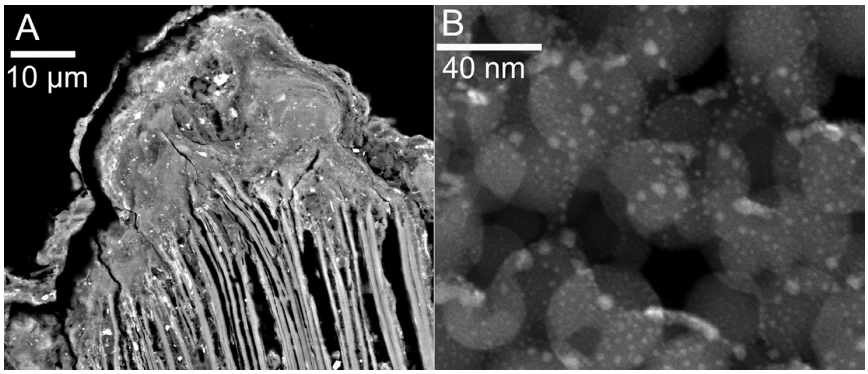

Fig. 6 Case hardening by silica glaze precipitation in a biotite grain, Akesu volcanic field, Tibetan Plateau. (A) BSE image of silica glaze that formed on top of a feathered biotite mineral grain. (B) HRTEM imagery of silica spheroids that have precipitated inside a pore space in weathering rinds. The silica spheroids composed of Si and O (Langworthy et al., 2010) are between 20 and 70 nm in diameter (right). Bright spots on the silica spheroids are artifacts of sample preparation.

The first nanoscale investigation of silica glaze formation revealed that silica precipitates in the form of spheroids with diameters between 20 and 70 nm (Langworthy et al., 2010) as seen in **Fig. 6**B. EDX analyses by Langworthy et al. (2010) indicate that these spheroids are composed of just Si and O. Spheroid diameter is particularly significant for interpreting the behavior of water at the nanoscale. There is a transition between complete and partial wetting on silica surfaces between 20 and 70 nm (Churaev, 2003; Zorin et al., 1992). This is the size range of the observed spheroids. Dorn (1998) originally suggested that crossing this transition ruptures the metastable wetting film (Zorin et al., 1992) resulting in silica precipitation—a hypothesis that is consistent with the presence of these spheroids (Langworthy et al., 2010).

Silica is an important case-hardening agent (Conca and Rossman, 1982; Dorn, 2004; Dorn et al., 2012; Gordon and Dorn, 2005a; Mottershead and Pye, 1994; Washburn, 1969; Wilhelmy, 1964; Robinson and Williams, 1992; Tratebas et al., 2004). Silica fills in voids in the weathering rind by growing new spheroids into pore spaces, since droplets "do not cling to a surface immediately after formation, but move somewhat before they attach to the [pre-existing] solid" (Koopal et al., 1999, p. 24). Thus, nanoscale silica instability explains silica-impregnation and subsequent case hardening of weathering rinds (**Fig. 6**).

While silica glaze is the most dominant case hardening agent, all rock coatings undergo dissolution and reprecipitation of the mobilized constituents into the underlying weathering rind. **Fig. 7** illustrates an example where rock varnish forms on a surface with abundant microcolonial fungi that dissolves varnish; thus, varnish is always growing and dissolving. The mobilized constituents reprecipitate inside the pore spaces of the weathering rind—much in the same way as silica glaze (**Fig. 7**B).

Rock coatings can also stabilize flaking rock surfaces by themselves, as exemplified in **Fig. 8**. The granitic clasts on many pediments and alluvial-fan surfaces in warm deserts undergo exfoliation (flaking) due to instability of the underlying weathering rind. It is common to see patches of rock surfaces darkened by the accumulation of rock varnish (**Fig. 8**). The BSE image in **Fig. 8** reveals that rock varnish stabilized such patches—at least temporarily. This sort of flaking and case hardening can occur in multiple cycles, where varnish reforms over a flaked surfaces that in turn case hardens the underlying weathering rind.

3.09.3.2 Tafoni

Tafoni (Paradise, 2013) can enlarge by a variety of processes that can involve internal moisture (Mol and Viles, 2012), temperature fluctuations (Hall and André, 2006), precipitation of carbonate and dissolution of primary mineral grains (Campbell, 1999), sea salts (Mottershead and Pye, 1994), and other rock-weakening processes. The location of rock detachment, however, has rarely been examined at the nanoscale.

Figs. 9 and 10 provide both micron-scale and nanoscale views of detachment of material inside a tafone in breccia (originally debris flows) and granodiorite, respectively. BSE imagery at the micron scale shows that several processes happen in tandem: dissolution increasing porosity; and mineral alteration and then physical separation are both occurring in the matrix of old debris flows (**Figs. 9**C and **10**B). Nanoscale imagery of the detachment of individual grains of debris-flow matrix (**Fig. 9**D) and biotite (**Fig. 10**C) suggest that detachment is a gradual process starting with a few nanometers of separation that then grows along a grain boundary and widens.

3.09.3.3 Arctic & alpine settings

Thermal stresses (Hall, 1999, 2006b; Hall and André, 2001, 2003; Hall and Thorn, 2011) and frost cracking (or frost wedging) (Van Vliet-Lanoë and Fox, 2018; Walder and Hallet, 1986) greatly influence cold climate geomorphic systems. The visual dominance of bare rock in alpine, arctic and Antarctic landscapes led to the paradigm that "physical weathering" dominates cold climates as

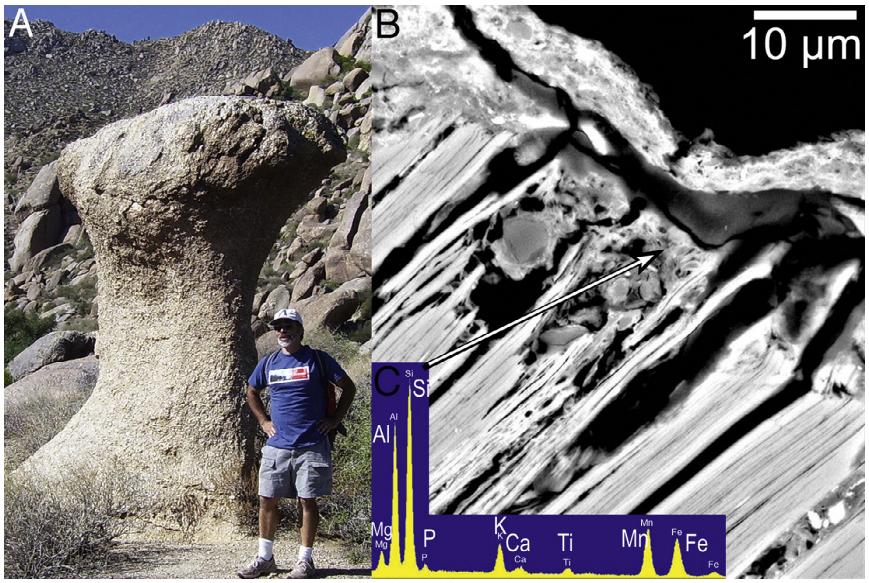

Fig. 7 Case hardening by mobilization and reprecipitation of rock varnish in the underlying weathering rind. (A) "Mushroom Rock" nubbin landform of the McDowell Mountains, central Arizona, USA that has its case hardened. (B) BSE image of the process of dissolution of the overlying rock varnish and subsequent reprecipitation inside the pore spaces—in this case a biotite mineral. (C) Energy dispersive spectra of the reprecipitated varnish, indicating a spectrum that is typical of subaerial varnish dominated by clay peaks (Mg, Al, Si), Mn, and Fe.

presented in physical geology and physical geography textbooks (Hobbs, 1919; Holmes, 1965; McKnight, 1993). Actual measurements in the mid-20th century, however, revealed the importance of chemical processes (Rapp, 1960). Hall (Hall, 1993; Hall and André, 2006; Hall and Otte, 1990; Hall and Thorn, 2011), Dixon (Campbell et al., 2001, 2002; Dixon, 1986, 2013, 2018; Dixon and Thorn, 2005; Dixon et al., 1984, 2002; Pope et al., 1995), Thorn (Thorn et al., 1989, 2001, 2006) and their collaborators followed Rapp (1960) in laying an empirical and theoretical foundation for dismantling the paradigm of the dominance of "physical weathering" in cold climates.

Nanoscale observations in cold climate settings ranging from Antarctica, to Greenland and the Tibetan Plateau fully support prior research highlighting the importance of chemical decay of rock and minerals (Dorn and Krinsley, 2019; Smith and Horgan, 2021). For example, quartz is generally through to be highly resistant to chemical reactions, especially in a cold and dry setting like the Tibetan Plateau, a perspective that is not supported by nanoscale observations. A free quartz sample from the Akesu volcanic field, for example, shows nanoscale roughness from dissolution (**Fig. 11**C), and this roughness plays an important role in the adherance of dust (**Fig. 11**A). Dorn and Krinsley (2019) also found nanoscale evidence of iron mobility, manganese mobility, as well as magnetite and plagioclase dissolution.

3.09.3.4 Splintering and nanoscale etching

Etching is a term used at almost all scales in geomorphology (**Fig. 1**), from etch plains that are erosion surfaces (Campbell and Twidale, 1991; Twidale, 2002), to etching that generates karst weathering forms in sandstone (Young, 1988; Young and Young, 1992), to etching of minerals in soils used as a relative dating method (Locke, 1979, 1986), to nanoscale etch pits generated by bacteria and analyzed by atomic force microscopy (Buss et al., 2007). In the context of mineral weathering, however, analyses of etch pit morphologies are traditionally carried out with secondary electrons and sometimes back-scattered electrons (Hall and Michaud, 1988; Lee and Parsons, 1995; White, 2005; Song et al., 2010), although they are sometimes studied at both the micrometer and nanometer scale (Brandt et al., 2003; Buss et al., 2007; Hochella and Banfield, 1995; Lee et al., 2007). As one would expect, isolated etch pits can be seen at the nanometer scale that "are typically only a few nanometers in depth and therefore not visible with SEM" (Brandt et al., 2003: 1457). Higher resolution nanoscale research reveals that the nanotexture of minerals, produced by defects dislocation densities and patterns, play a key role in how minerals decay (Banfield and Barker, 1994; Brown and Lee, 2007; Hochella and Banfield, 1995; Lee et al., 2007).

Studies of mineral etching at the nanoscale have raised a critically important conundrum with respect of clay mineral production by chemical weathering. Decades of thought about mineral weathering generated a paradigm that feldspar chemical weathering always leads to clay mineral production, as supported by some of the first nanoscale weathering studies of feldspars (Banfield and Eggleton, 1990). More recent research, however, reveals that water to rock ratios in the weathering environment may be

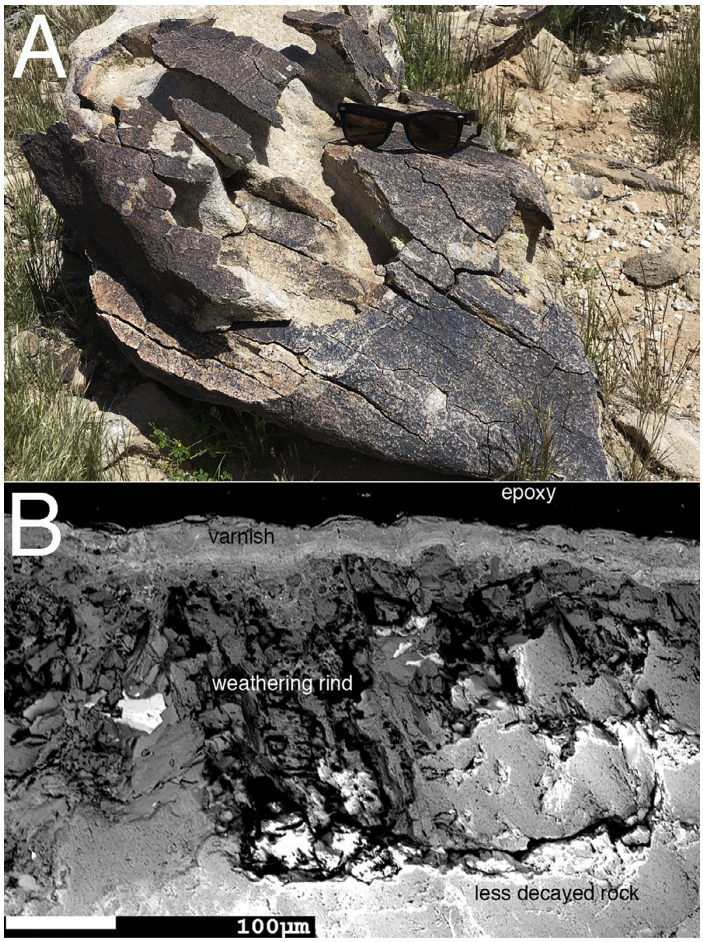

Fig. 8 Case hardening of a pediment core stone, Maricopa Mountains, Arizona, USA. (A) The granitic material of the underlying rock is undergoing flaking due to porosity destabilizing the weathering rind. (B) In places, however, the surface has been stabilized by the accretion of rock varnish as seen in this BSE image.

a key determinant in whether or not clay mineral alteration products are found at the nanometer scale (Lee et al., 2007). In other words, clay minerals do not always occur next to feldspar minerals; the nanoscale weathering environment is an important player, especially via capillary scale and nanoscale water.

The scale jump connection between mineral nanoetching and much larger forms has not been considered in the literature, according to our understanding. However, we believe that making such a linkage is possible and propose here a speculative connection between nanoetching and the weathering form termed "splintering" (Dorn et al., 2008; Fitzner and Heinrichs, 2004; Fitzner et al., 1997; Stoppato and Bini, 2003). Splintering is where all different types of rocks, from basalt to sandstone to schist to granite, have the appearance of pages of a book that has been wetted and then dried (**Fig. 12**).

In the case of a foliated metamorphic rock, where grains are aligned, the weathering form of splintering is likely a consequence of differential weathering of more susceptible minerals at the micrometer to millimeter scale. Splintering simply reflects the millimeter to centimeter expression of micron-scale processes (**Fig. 13**). However, splintering is a ubiquitous weathering form in virtually all rock types, even those with no obvious alignment of minerals. Explaining how this takes place at the hand-sample scale has not been a topic of focus in the geomorphic weathering literature.

Our hypothesis that relates splintering forms (**Fig. 12**) to the nanoscale alignment of etching is that subparallel alignment of mineral etching at the nanoscale can lead to alignment of capillary water conduits at the micrometer and then millimeter scales. These capillary water conduits appear to be key agents for the propagation of mineral weathering (Meunier et al., 2007).

Evidence in support of this hypothesis is presented in **Fig. 14**, a case study of a silicified dolomite from South Australia, where the alignment of splintering at the hand sample scale corresponds with dissolution of microfractures carrying capillary water at the micron scale, and then also with alignment of connected weathered pores at the nanoscale. Nanoscale alignments appear to enable

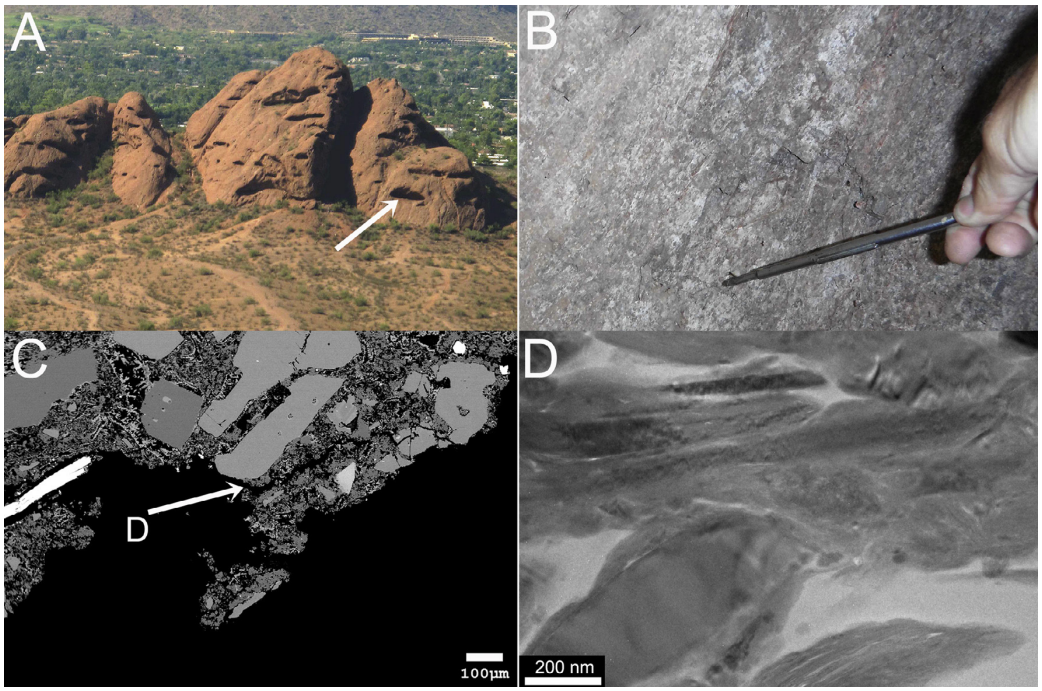

Fig. 9 Tafone enlargement through nanoscale detachment at Papago Park, Phoenix, USA. Image (A) illustrates a pediment and inselberg complex composed of breccia that originated as debris flows, where the arrow points to the sampled tafone. (B) Sampling location at the rear of the tafone. (C) Micron-scale BSE image showing how the silty-clay matrix of the debris-flow breccia separates and allows detachment, where the small D indicates the location of the HRTEM image. (D) HRTEM image showing particles in the matrix of the debris-flow breccia that are separating from one another. This separation is just a few nanometers at first, but grows until a fracture can be seen at the micron scale.

propagation of capillary water-bearing fractures in subparallel alignments that in turn generated the splintering weathering form seen at the hand sample scale. By way of analogy, this conceptual model is similar to the way a parallel drainage pattern develops through taking advantage of fracture patterns.

3.09.4 Nanoscale processes as a limiting factor in erosion

Geomorphologists have long been aware of the importance of rock decay in limiting rates of erosion. G.K. Gilbert introduced the notion of a "weathering-limited" landscape of (Gilbert, 1877) bare-rock landforms. Gilbert's concept differs from a more popular and more recent derivative of a detachment-limited condition (Ahnert, 1976). Gilbert (1877: 105) explained that "in regions of small rainfall, surface degradation is usually limited by the slow rate of disintegration; while in regions of great rainfall, it is limited by the rate of transportation."

Rather than trying to measure Gilbert's (1877: 105) "rate of disintegration," geomorphologists tended toward measuring "detachment-limited" systems (Howard, 1994). Howard (1994: 2261–2262) noted that the rate of transport of weathered materials is "limited by the ability of the flow to entrain or erode regolith (residual soils or colluvium) or bedrock, giving 'detachment-limited conditions'." Thus, detachment-limited systems can be analyzed through sediment transport measurements over short timescales (Howard, 1994), while cosmogenic nuclides measure bedrock detachment rates over longer timespans (Seong et al., 2016a).

The first part of this section focuses on the importance of nanoscale processes in controlling Gilbert's weathering-limited processes of disintegration operating in warm deserts, while the second part of this section explores an example of how nanoscale processes influence Ahnert's detachment-limited erosion in the context of pediment and strath erosion in granitic materials of the Sonoran Desert, Arizona, USA.

3.09.4.1 G.K. Gilbert's weathering-limited landscapes

Fractures found in Earth's rocks originate through rock-forming processes and tectonic deformation (Ehlen, 2002; Engelder, 1987; Eyles et al., 1997; Hobbs, 1967; Molnar et al., 2007; Schultz, 2000; St Clair et al., 2015; Twidale and Bourne, 1978). These fractures, or joints, influence geomorphic processes and forms across different scales (Scheidegger, 2001; Scott and Wohl, 2018). Although

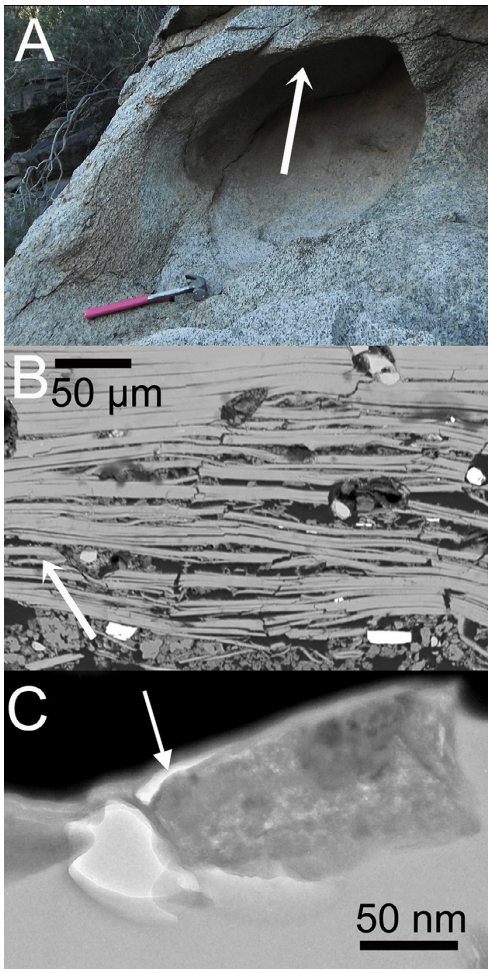

Fig. 10 Tafoni enlargement through nanoscale detachment at South Mountain, Sonoran Desert, Arizona, USA. Image (A) shows a tafone developed in granodiorite, with the arrow identifying the location of detaching materials along the roof. (B) The roof position is at the top of this BSE image with relatively fresh biotite. Mineral alteration, increase porosity, and physical separation occurs in tandem. The arrow indicates the location of the HRTEM image in (C). (C): HRTEM image where the black material is mineral material too thick for electron transparency. Altered biotite that is thin enough for electron transparency just barely separated as revealed by the white strip (arrow).

fracture widening and lengthening can occur by a variety of erosive processes (Scott and Wohl, 2018), rock decay by physical and chemical processes plays a key role in fracture propagation—often leading to rock detachment.

Three general types of rock-decay processes physically wedge open fractures through frost cracking (or frost wedging) (Walder and Hallet, 1986), roots and their associated fungi (Brantley et al., 2017; Gadd, 2007; Merrill, 1906), and dirt cracking (Ollier, 1965). Dirt-cracking fines found inside rock fissures are not skeletal or embryonic soils (Certini et al., 2002; Darmody et al., 2008) or fills found in *in situ* decayed rock (Frazier and Graham, 2000; Thoma et al., 1992). While the first two fracture-wedging processes are generally well known and generally taught in introductory courses, dirt cracking is rarely taught.

Originally proposed in Australia as an insolation-related process (Ollier, 1965), experimental evidence and electron microscope studies revealed that the widening of fractures due to dirt cracking in warm deserts relates to two complementary processes (Dorn, 2011): first, calcrete precipitation wedges open fractures wide enough so that desert dust can begin to accumulate; second, wetting and drying of the desert dust then widens fractures to the point where spalling occurs (Dorn, 2011; Ollier, 1965). Dirt cracking leaves behind a visible signature, because the dust inside fractures promotes the development of an iron film on the walls of the fracture, while the laminar calcrete often leaves behind a whitish coating (**Fig. 15**).

The ubiquitous dust in warm deserts (Bullard and Livingston, 2009; Goudie, 1978) and laminar calcrete (Chitale, 1986; Coudé-Gaussen et al., 1984; Koning and Mansell, 2017; Shtober-Zisu et al., 2018; Villa et al., 1995) moves deeper into fractures, and dirt cracking eventually leads to erosion of bedrock desert landforms at rates ranging from 0.17% to 1.12% of a surface spalled every

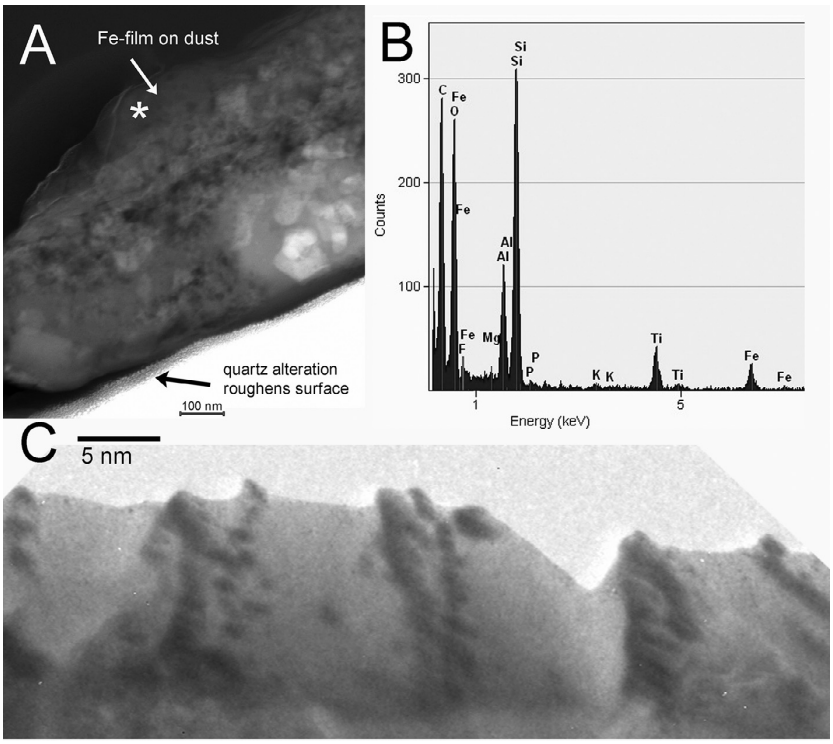

Fig. 11 Alteration of free quartz on the surface of a lava flow, Akesu volcanic field, Tibetan Plateau. (A) A dust particle adheres to the quartz surface that maintains a roughness from nanoscale dissolution. Note the bumpy appearance of the quartz. The dust particle has adhered to the surface long enough to accumulate a titanium-iron-rich film (B) EDX analysis of the iron-rich film that is composed of mostly Si and Al, but with major amounts of Ti and Fe. (C) The very surface of the quartz has a microtopography that appears to be dissolution grooves.

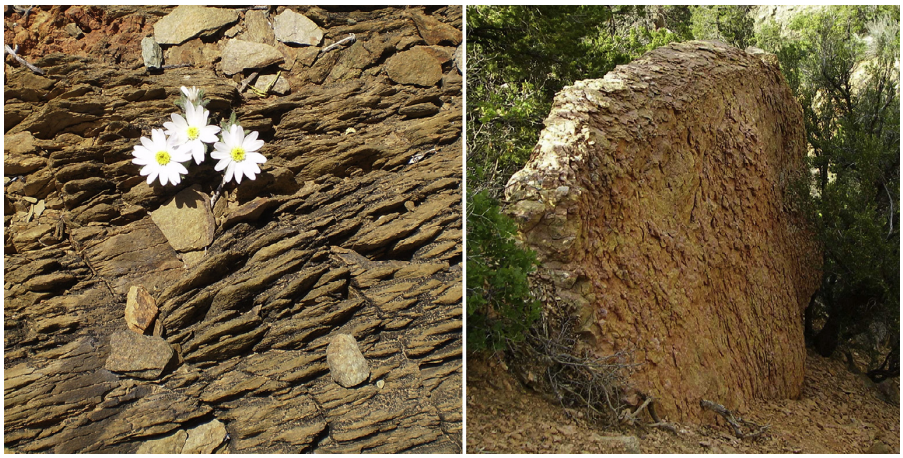

Fig. 12 The weathering form of splintering seen at a hand specimen scale (left, where the flower width is 2 cm) and where the talus boulder is 2 m tall (right). Left image is of a hornfel at Black Canyon, Arizona; right image is of sandstone at Bryce National Park, Utah.

thousand years (Dorn, 2018); thus, the dirt-cracking process alone is able to completely resurface desert bedrock landforms such as bornhardts in 165–600 ka, cliff faces composed of basalt and other resistant rocks in 139–417 ka, and slick rock in ~93 ka (Dorn, 2018).

Dirt cracking can be studied at a variety of spatial scales. At the field scale, areas of detachment can be mapped and quantified (Dorn, 2018). At the micron scale, the processes of dust infiltration and laminar calcrete precipitation can be analyzed through

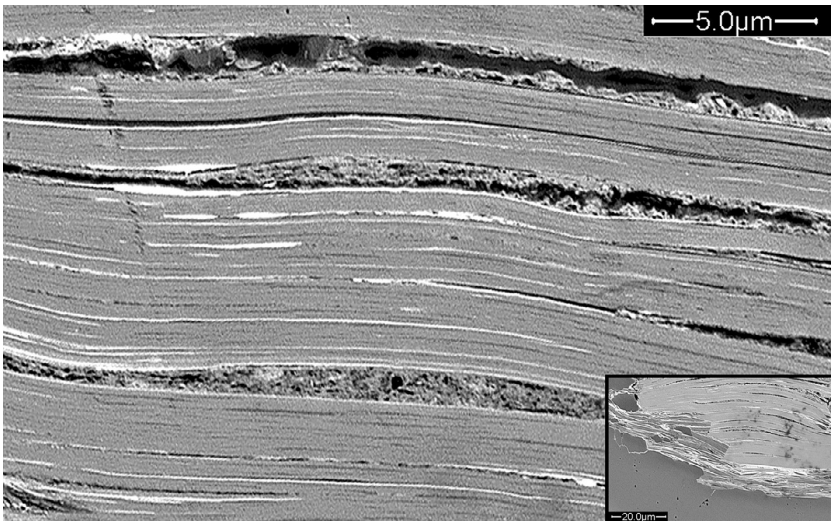

Fig. 13 BSE image of biotite from a gneiss clast in a desert pavement near Florence, Arizona, undergoing a mix of splintering and grussification. The main aspect of this image feature is that the biotite itself has expanded volumetrically. Some of this expansion is due to the formation of secondary weathering products, such as the bright iron oxides or the darker material rich in silicon and aluminum. The inset image shows the broader context of biotite next to quartz, and how the biotite weathering breaks bonds among different minerals in the rock.

back-scattered electron microscopy and energy dispersive X-ray spectrometry (**Fig. 16**). However, it is at the nanoscale where the fissure wedging can be best observed (**Fig. 17**).

Quantitatively, dirt cracking is the single most important physical weathering process yet known in warm deserts (Dorn, 2018). This statement is true, in part, because no other physical weathering process has yet been measured in terms of its influence in resurfacing weathering-limited bedrock landforms. Ultimately, however, the rate of dirt cracking is limited by the rate of nanoscale processes widening fissures to the point of detachment.

3.09.4.2 Detachment-limited pediment & strath erosion

Larson and co-workers studied processes and rates of granitic landform development in the Sonoran Desert (Larson and Dorn, 2014; Larson et al., 2014, 2016; Seong et al., 2016b). A key-limiting factor in rates of erosion of granitic pediments (e.g., **Fig. 18**) and granitic straths is the detachment of grus (granitic minerals) from bedrock.

For pediments adjusting to base level changes (e.g., **Fig. 18**), erosion requires that the granitic bedrock be in a sufficient state of decay to enable detachment (Larson et al., 2016). Using the BSE technique discussed in **Section 3.09.2**, Larson et al. (2016) used the ratio of porosity in the incising channel to the porosity in bank materials as a proxy for erodability of bedrock. Banks that have less porosity are more resistant to erosion than channel floors and produce narrow incising washes (e.g., Mine Pediment in **Fig. 18**). In contrast, more decayed banks allow channels to widen and plane the pediment (e.g., Bush Pediment in **Fig. 18**). **Fig. 19** illustrates the nature of granitic decay that leads to grussification and enables pediment erosion.

Concomitantly, analyses of ephemeral granitic drainages at South Mountain, Phoenix, USA, indicates that strath widening also requires mineral decay. Micron and nanoscale electron microscopy reveals that grussification of granitic bedrock in straths of even small washes occurs primarily through abiotic biotite oxidation and also biotic processes associated with mycorrhizal fungi and roots of plants growing along wash banks (**Fig. 20**). Ultimately, rates of strath widening are limited by long-term rates of decay of granitic minerals to the point where physical detachment can occur.

3.09.5 Nanoscale biological mineral decay

3.09.5.1 Ants as agents of carbon dioxide sequestration

Rising levels of atmospheric CO_2 and other greenhouse gases have been a major focus of interest in the late 20th and 21st centuries. Under natural conditions and over geological timescales, dissolution of calcium and magnesium silicates have played a major role in the sequestration of carbon dioxide through the precipitation of limestone and dolomite (Brady, 1991). Abiotic dissolution of Ca-Mg-silicates is much slower than dissolution influenced by biological agents; the biotic enhancement of weathering (BEW) has promoted global habitability (Schwartzman, 2002, 2017; Schwartzman and Volk, 1989) by accelerating rates of CO_2 sequestration. A quarter-century of monitoring samples extracted every 5 years from ant colonies reveals that ants may be the single most powerful

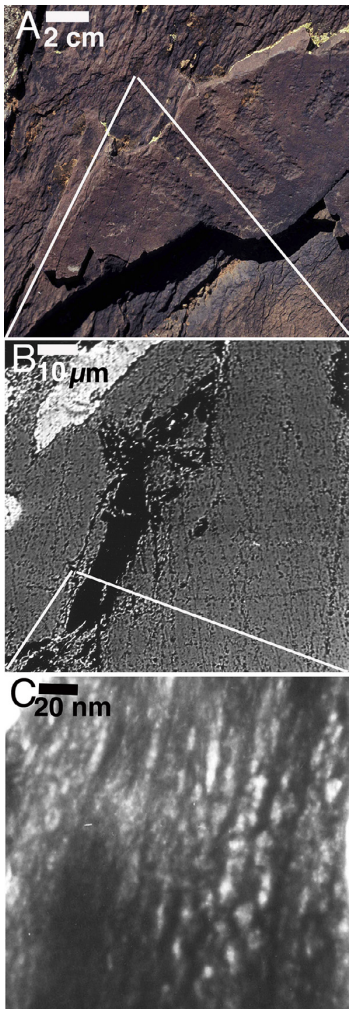

Fig. 14 The weathering form of splintering of a silicified dolomite, South Australia (A—hand sample scale), appears to correspond with the development of aligned micron-scale fractures that carry capillary water (B—micron scale BSE image), and in turn with the alignment of nanoscale pores that are connected (C—nanoscale HRTEM image) and could be responsible for fostering the growth of micron-scale fractures. Lines indicate locations of sample collection for analysis at progressively finer scales.

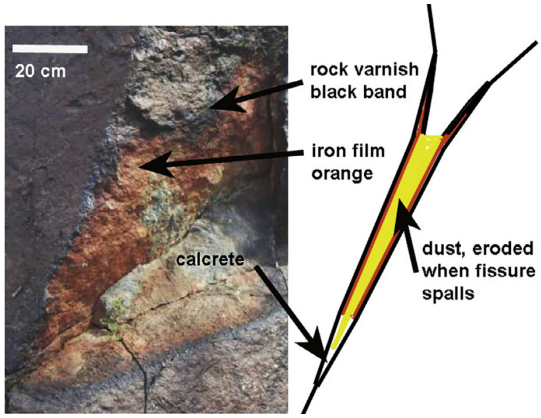

Fig. 15 This fissure once hosted eolian dust and some weathered rock fragments that were washed away prior to photography. The innermost side of the opened fissure is coated is with laminar calcrete. The outer few centimeters are coated by a ring of black rock varnish. The remainder of the fracture side is covered by orange iron film.

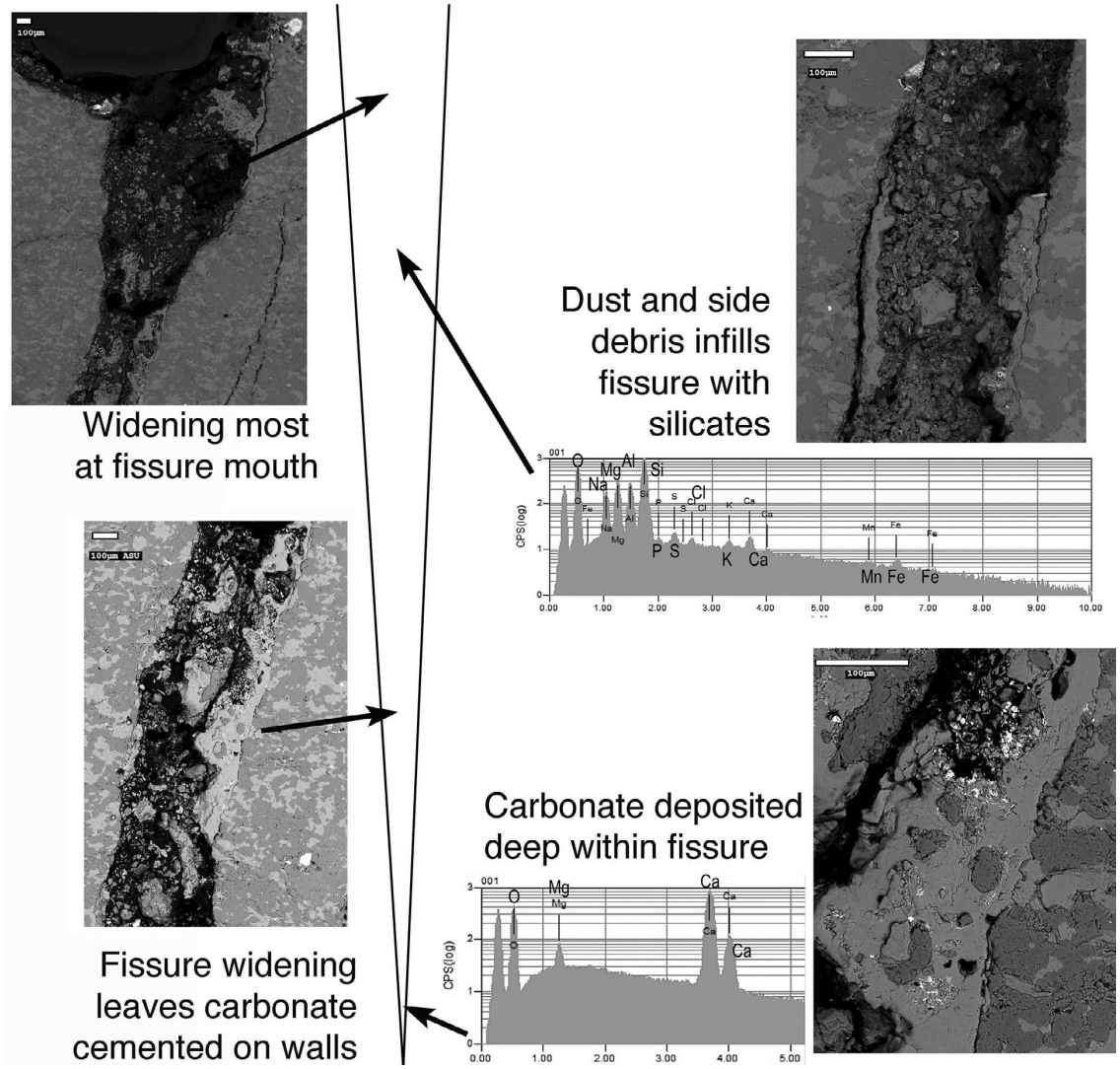

Fig. 16 Fracture enlargement by dirt cracking. The "V" in the middle of the diagram is an idealized rock fracture where the different samples were collected to analyze dirt cracking. Ubiquitous fractures in warm deserts, such as this sample collected from Papago Park, Phoenix, USA, display a general sequence illustrated by micrographs taken at different depths. An idealized fracture contextualizes the depths at which the images were acquired. In this case, the fissure length was 5 mm. To preserve *in situ* relationships, the fissure was first filled with epoxy in the field prior to mechanical sampling. The scale in each micrograph is 100 μm in length. Top Position in Fissure: the fissure opens its widest at the intersection of the fissure and the inside of a tafone. Black epoxy indicates an abundance of void space, but some infilled debris eroded from the rock along sidewalls mixes with dust. Second Position in Fissure; silicate-dominated dust and rock debris (according to EDS spectra) fill in fractures a millimeter underneath the opening. Third Position in Fissure: as the fissure penetrates more into the host rock, carbonate, rock material from the side walls, and dust intermix. Deepest within the fissure: carbonate (calcium and magnesium carbonate, according to EDS Spectra), carbonate fills almost the entire fracture. Ongoing mobilization and reprecipitation appears to be the process by which fractures deepen.

agent of natural carbon sequestration; Ca-Mg-silicates placed in colonies of different ant species dissolved at rates 50x–300x controls, much faster than Ca-Mg-silicates placed in termite colonies or even root mats (Dorn, 2014).

Schmeeckle et al. (2021) investigated a possible mechanism by which ant colonies greatly enhance BEW. They took an aqueous solution derived from crushed California harvester ants (*Pogonomyrmex californicus*) and used atomic force microscopy (AFM) to measure dissolution directly. The whole ant extracts (WAE) greatly accelerated rates of Ca-feldspar dissolution, supporting the assertion that ants can act directly as BEW agents (Schmeeckle et al., 2021). They observed visible effects (e.g., **Fig. 21**) just 6 h after WAE was placed on polished surfaces of plagioclase feldspar samples.

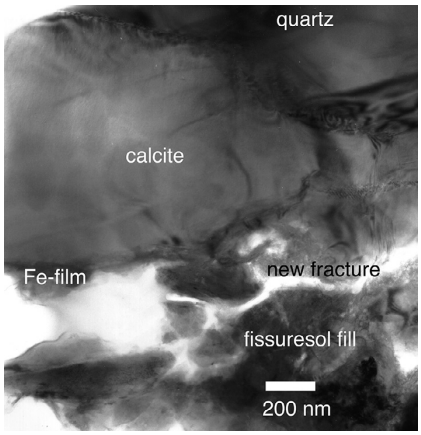

Fig. 17 HRTEM image of a fracture at South Mountain, Phoenix, USA. The rock fissure side (quartz) is at the top. Wedging of the fissure occurred in a series of superimposed events starting with laminar calcrete deposition (calcite) on top of the quartz, followed by an iron film developing on the calcrete, and then by fill deposited in the fissure. Then, the fracture continued to widen, developing a newer fracture. EDX analyses determined the composition of these materials.

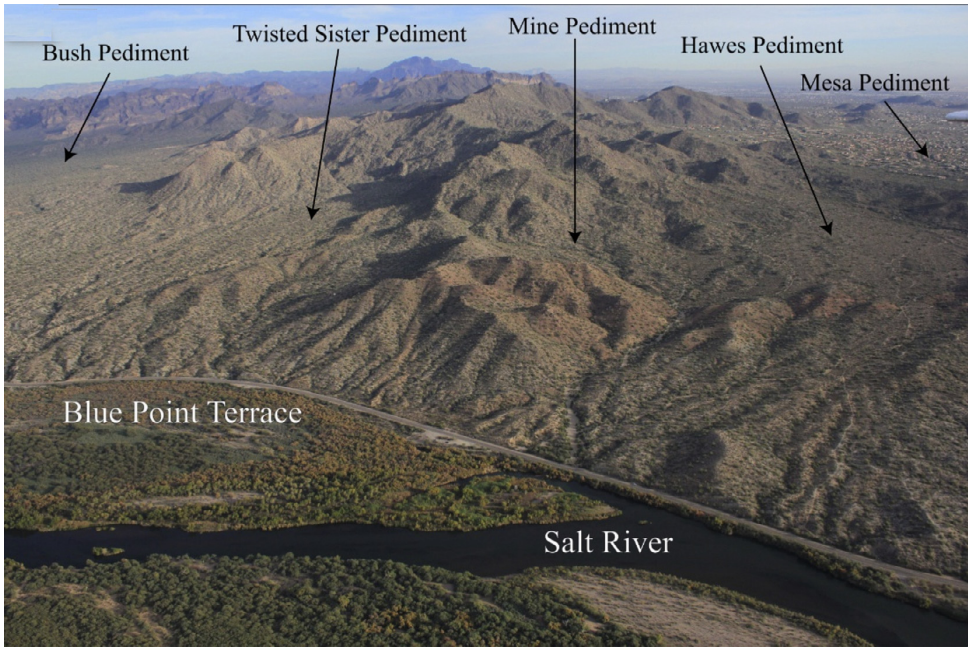

Fig. 18 Low angle SE-looking aerial photograph of the Usery Mountains, Sonoran Desert, Arizona, and different pediments. Note the varied topography on each pediment with varying levels of incision in response to the base level lowering of the Salt River. The Mesa Pediment grades to the ca. 90 ka Mesa Terrace level to the right of this photograph. The other pediments have responded to the base level lowering of the Salt River and have varying degrees of incision, with the Bush Pediment being almost completely regraded to the ca. 40 ka Blue Point Terrace. Also, note the escarpment at the base of the pediments resulting from lateral migration of the Salt River into the pediment basins.

A newly recognized form of calcium carbonate, hydrated crystalline calcium carbonate, is a product of biomineralization (Zou et al., 2019). When a plagioclase (Ca-silicate) grain was examined from the *Pogonomyrmex* ant nest, Palo Duro, West Texas from the 25-year study (Dorn, 2014), the texture of calcium carbonate had the same appearance as the hydrated crystalline calcium carbonate identified by Zou et al. (2019) (**Fig. 22**).

Further nanoscale evidence for the importance of ants in promoting the dissolution of Ca-silicates comes from a study of a polished cross-section of Hawaiian basalt placed in the same *Pogonomyrmex* ant nest, Palo Duro, West Texas (Dorn, 2014). A polished cross-section was removed from the field after 10 years and examined for changes. Ground control points (epoxy dots)

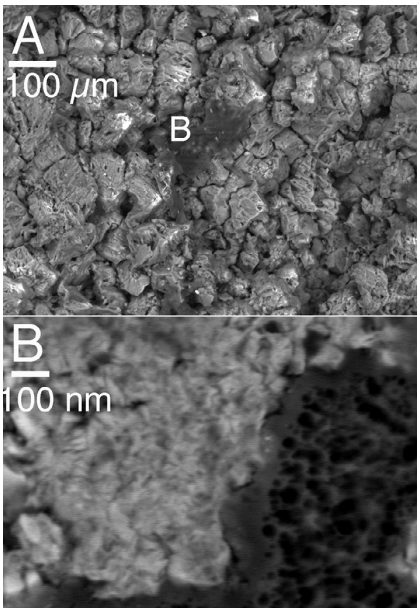

Fig. 19 Images of granitic decay of the Usery Mountains pediments, Sonoran Desert, USA. Pediments that are undergoing both incision and lateral planation by washes have undergone substantial grussification to weaken grain-to-grain cohesion. (A) Secondary electron image showing fracturing along internal weaknesses in mineral grains that is characteristic of grussification at the micron scale. Much of the grussification is due to dissolution producing enhanced porosity. Some is due to mineral grain alteration, as seen at the location of the letter B. (B) BSE nanoscale image showing an altered grain of hornblende next to a plant root (that has a darker and more porous texture).

helped relocate different spots on the cross-section. Fig. 23 exemplifies the sorts of plagioclase etching that occurred in the ant colony after just 10 years. The pitting process appears to involve both dissolution of plagioclase and alteration to clay minerals. Gentle washing of the cross-section dislodged most of the alteration products, but some clays can be seen at nanoscale resolutions (Fig. 23C).

3.09.5.2 Biological processes and the fallacy of Goldich's weathering sequence

The generally accepted view is that mineral weathering proceeds along the reverse of Bowen's reaction series that explains mineral crystallization. The weathering sequence published by Goldich (1938) is the opposite of Bowen's sequence. It starts with the weathering of olivine, since olivine formed at the hottest temperatures, and ends with quartz being one of the most stable minerals because it formed last at the coolest temperatures. Research on biotic mineral and rock decay over the past several decades continues to reveal its importance at Earth's surface by such agents as fungi (Gadd, 2007, 2017; Li et al., 2016; Wild et al., 2021), and also far below as microorganisms are found at great depth in Earth (Reith, 2011). Biological processes, and not thermodynamics, may explain why Goldich's weathering sequence is valid in some conditions and locations.

An unstated but critical assumption in Goldich's thermodynamic interpretation was discovered through field-based research using BSE to study the surfaces of lava flows of Hualalai, Hawaii. This research revealed that olivine does not weather first (Wasklewicz, 1994; Wasklewicz et al., 1993;), as predicted by the Goldich weathering sequence (Goldich, 1938). The field sites where olivine weathered last, not first, had a paucity or organic acids—being located in the rainshadow of both Mauna Loa and Hualalai. Olivine was much less weathered than plagioclase and clinopyroxenes in those lava flow surfaces devoid of acid-producing lichens and fungi and distant from vegetation. In contrast, olivine weathered much faster at lava flow surfaces that hosted acid-producing organisms. Nanoscale research may hold the key to explain the apparent contradiction between Goldich's (1938) sequence and the observations from the rainshadow of Hawaii.

Goldich's (1938) original field sites were located in a humid environment that contained abundant organic acids and organisms. Other workers have confirmed Goldich's sequence in similar humid environmental settings (Velbel, 1993). A working hypothesis is that Goldich's weathering sequence could be more a function of biotic weathering environment than the thermodynamics of mineral formation.

An important biotic influence on the sequence of mineral weathering could be microbial weathering. Laboratory research on bacterial weathering at the micron-scale determined that Goldich's weathering sequence is in accord with the vulnerability of

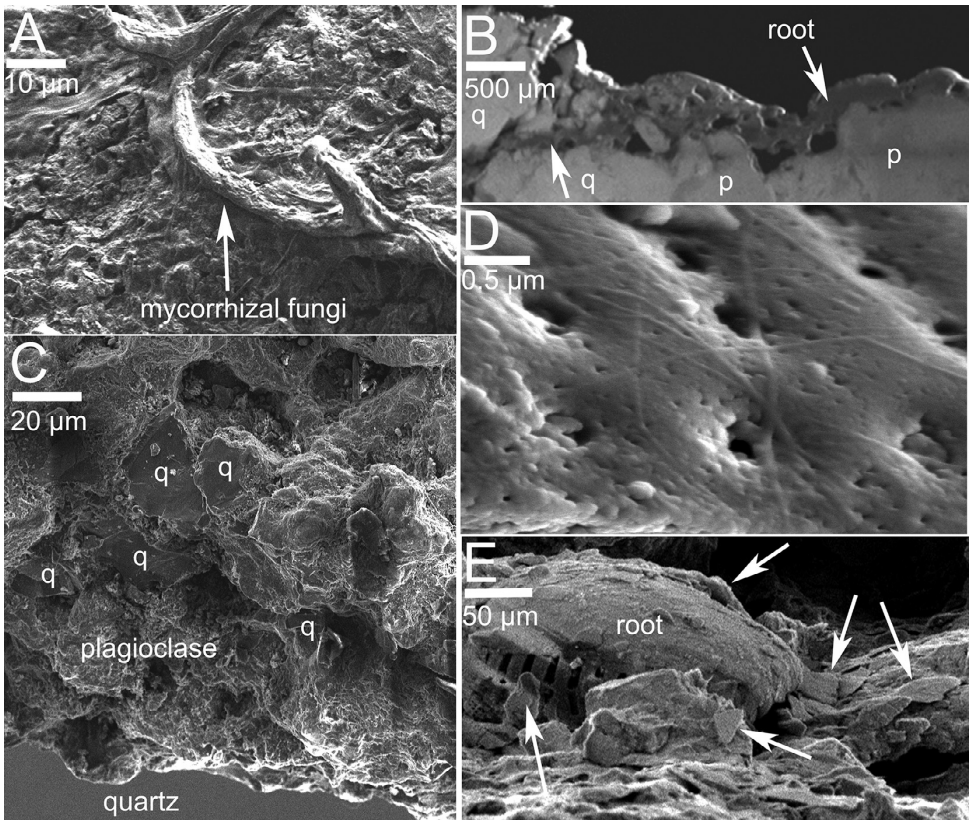

Fig. 20 Secondary electron images of rock decay along banks fronted by hard-rock straths. The images all show the effects of mycorrhizal fungi (image A) and roots (B). Mineralogy (q = quartz; p = plagioclase) is based on EDX analyses. Most of the effect appears to be the decay of plagioclase grains to the point where they have very little internal cohesion. Image (C) highlights this where the relatively intact quartz contrasts with the thoroughly disintegrated plagioclase. However, quartz also decays, as exhibited by nanoscale dissolution pits in image (D), where the pits are visible because the mycorrhizal fungi were removed. The lines on the quartz surface have the same EDX Si and O signature as the quartz, and thus they could reflect redeposition of silica. Image (E) shows that the process of decay can involve physical force breaking apart minerals, as evidenced by the angular particles (arrows) of quartz found in abundance in physical proximity to the root. Scale bars are in micrometers.

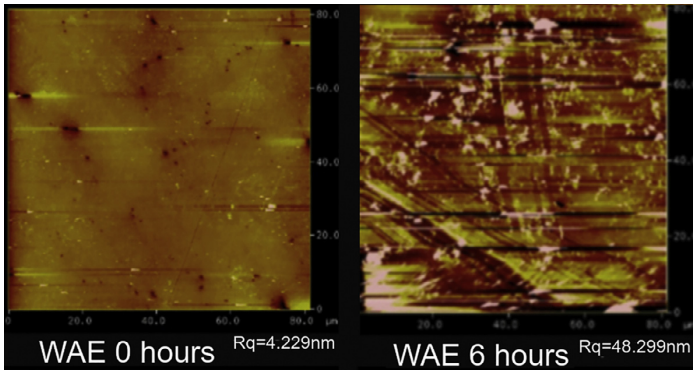

Fig. 21 A comparison of a polished plagioclase surface before application of a whole ant extract (WAE) solution and after application for 6 h. Rq is a measure of surface roughness used in AFM studies, and Schmeeckle et al. (2021) found a highly statistically significant difference between the control (WAE 0 h) and just 6 h of WAE. NOTE: the horizontal streaks are an artifact of the AFM analysis.

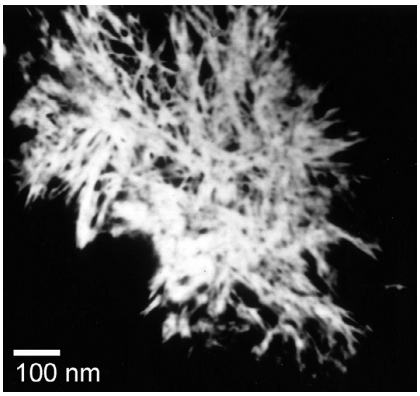

Fig. 22 BSE image of a precipitate on a plagioclase grain extracted from an ant nest after 20 years. EDX analyses identified the material containing calcium, carbon and oxygen and hence most likely as calcium carbonate. This texture is the same as biogenic hydrated crystalline calcium carbonate.

minerals to bacteria (Song et al., 2010). One possible reason for microbial activity causing the Goldich sequence could be the nutrient needs of microbes (Bennett et al., 2001):

> A basic tenet of sediment diagenesis, the "Goldich Weathering Sequence" (Goldich, 1938), states that the most unstable silicate mineral will weather (dissolve) first, with more resistant silicates taking progressively longer to dissolve (from least to most stable), olivine < plagioclase - < albite < anorthoclase < microcline < quartz. The observed weathering sequence of minerals in an anaerobic, microbially controlled system, however, is almost opposite, with olivine stable with respect to microcline, and the relationship between microbial colonization and weathering rate almost perfectly correlated. This suggests that, in some environments, the indigenous microorganisms may significantly alter weathering patterns as they aggressively scavenge limiting nutrients.
>
> Bennett et al. (2001: 16)

Another nanoscale explanation for the discrepancy between Goldich's sequence and weathering in abiotic contexts (Barker and Banfield, 1996) follows:

> Biologically mediated weathering involves a complex dissolution/selective transport/recrystallization mechanism occurring within the acidic extracellular gels coating all mineral surfaces. A specialized weathering microenvironment around each mineral grain initially produces minute phyllosilicate crystallites. A rind of clay minerals forms around the dissolving parent phase, eventually culminating in abundant 5–10 μm diameter polymer-bound aggregates of face-to-face oriented clay minerals of homogeneous composition. Physiochemical weathering of ferrohastingsite produces topotactically oriented smectite and goethite. The cleavage-controlled reaction is neither isochemical nor isovolumetric.

A sub-40-nm scale study of microbial weathering of a Mg-Fe-pyroxene in a meteorite that was exposed to weathering for about 70 years (Benzerara et al., 2005a, 2005b) provides additional insight. Microbial interactions over seven decades led to carbonate precipitation in the form of rod-shaped nanocrystals of calcite and the development of an amorphous Al-rich layer—all leading to the conclusion that microorganisms create nanoscale weathering environments that dramatically alter weathering. Micron- and nanoscale studies of fungi and bacteria weathering of an exposed granitic pegmatite similarly stresses the importance of microbial ecology in subaerial settings (Gleeson et al., 2005, 2006).

One possible way that microorganisms might affect weathering is through interactions with fungal hyphae (Wild et al., 2021). Nanoscale *in situ* observations of a soil fungus interacting with biotite over 3 months revealed a nanoscale attachment to the mineral. Biomechanical forcing altered interlayer spacings, and microbial processes leached potassium, all leading to the formation of vermiculate and clusters of oxidized iron (Bonneville et al., 2009; Smits et al., 2009).

These clusters of iron oxides are features commonly seen in BSE images of weathering rinds at the micron scale (Pope et al., 1995), as illustrated in **Fig. 24**. One nanoscale hypothesis for this ubiquitous weathering-rind phenomenon of submicron fragments of iron oxide could be the ubiquitous presence of fungal hyphae.

Linking micrometer and nanoscales at the hand sample level requires more than examination of just a few samples. However, pilot investigations of randomly selected samples do have the potential to suggest future research directions. A sample from the Hawaii BSE study of olivine weathering (Wasklewicz, 1994; Wasklewicz et al., 1993) was reevaluated with HRTEM. This sample was collected from a Hualalai Volcano basalt flow f5d c8.2 (~2000 years old) ad was covered with lichens. As in prior research (Bonneville et al., 2009), hypha appear to be able to exert enough pressure to split apart smectite clays in the weathering rind (**Fig. 25**A).

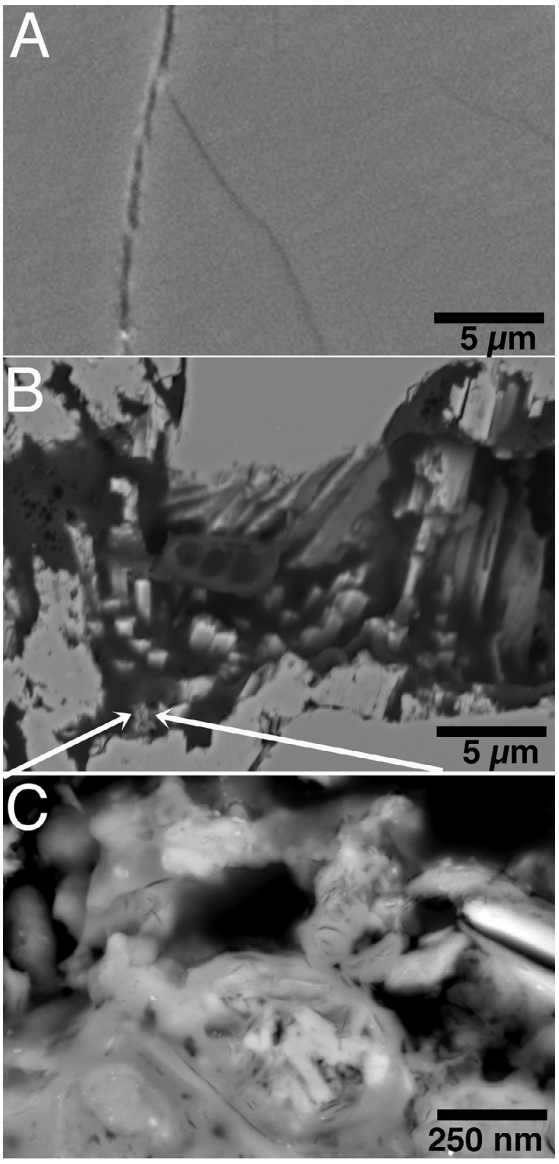

Fig. 23 Ten years of exposure to a *Pogonomyrmex* ant colony, Palo Duro, West Texas. (A) BSE image of the studied cross-section before emplacement in the ant colony. (B) BSE image of the same location as image (A), but after 10 years of exposure. The object in the middle of the frame with three cellular-like structures is the right size to be fungal material. Note that the various cleavage planes in the plagioclase have nanoscale dissolution pits. An overall lack of weathering products such as clays is probably from gentle washing of the sample. Still, some weathering products were not removed. The arrows point to the location of image (C). (C) BSE image at the nanoscale showing clays produced by *in situ* decay of the plagioclase.

As in prior research on bacteria weathering (Hiebert and Bennett, 1992), fungal hypha appear to be able to extract particular elements. Instead of potassium extracted from biotite (Bonneville et al., 2009), there is an uptake in calcium (**Fig. 25**). EDX analyses reveal that there are strings in the imagery in **Fig. 25**. These linear strings appear to be rich in calcium. The apparent source of the calcium appears to be an olivine grain. The reason for this uptake is uncertain. The calcium might be used in the formation of calcium oxalates produced by many lichen (Bjelland and Thorseth, 2002; Wadsten and Moberg, 1985) and fungi (Smits et al., 2009), or calcium might be used in another microbial process. Regardless of the need, nanoscale fungal weathering of olivine could provide yet one more explanation why Goldich's weathering sequence depends upon the presence of organisms and is incorrect where there exists minimal contact between minerals and biotic activity.

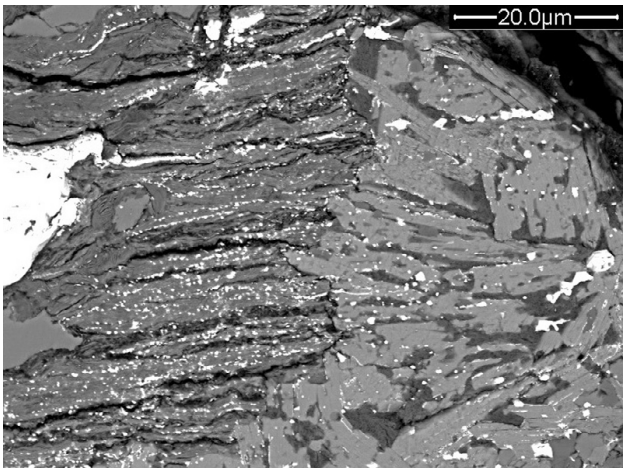

Fig. 24 Cross-section of the weathering rind of a metamorphic schist in the Phoenix Mountains, central Arizona. The bright mineral on the far left side is magnetite. Muscovite is the middle mineral, and hornblende is on the right side. Sub-micron clusters of iron oxides have precipitated throughout the muscovite and even into the hornblende. Iron mobilized from biotite has been observed to fracture rocks in Karkevagge (Dixon et al., 2002).

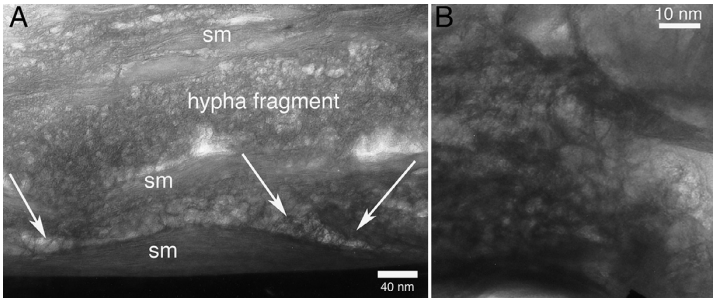

Fig. 25 Fungal hyphae appear to be extracting calcium from olivine in the weathering rind of a Hualalai basalt flow covered by lichen. (A) Overview of the interface of a hypha (granular appearance), smectite clay (sm), and an olivine mineral (dark, thicker and hence electron opaque at the bottom). Arrows show nanoscale strings of darker material that show a spike in calcium in energy dispersive measurements. Given that the lower end of typical hypha diameter is ~2 μm, it is possible that this cross-section shows an undulating hypha surface surrounded by smectite clay (B). Close-up of the boundary between hyphae nanoscale strings of calcium and the underlying olivine (dark, thicker, electron opaque at lower left).

3.09.6 Nanoscale processes and dust generation

Silt in the form of dust is ubiquitous on Earth (Bullard and Livingston, 2009; Goudie, 1978), Earth's moon (Gaier, 2005), Mars (Israel et al., 1997) and likely elsewhere. Weathering interactions within dust and between dust and underlying mineral surfaces are taking on increasing importance in understanding the decay of building stones (McAlister et al., 2006; Sharma and Gupta, 1993; Smith et al., 2007), formation of rock coatings on earth (Dorn, 2009; Krinsley et al., 2009) and Mars (Johnson et al., 2002; Kraft et al., 2004), in understanding historic and prehistoric archaeology (Ganor et al., 2009), and in Quaternary research (Kleber, 1997; Yaalon and Ganor, 1973). Nanoscale research informs on dust production (Hochella, 2002a; Pye, 1987, 1989) and also what happens when dust deposits on rock surfaces as dust films and components of rock coatings.

There is evidence that silt production is a function of inherent weaknesses in minerals such as quartz (Kumar et al., 2006; Moss and Green, 1998; Smalley et al., 2005), as well as external processes such as salt weathering, abrasion, frost weathering (Smalley and Krinsley, 1978; Whalley et al., 1982; Wright et al., 1998), microbial weathering of quartz surfaces (Brehm et al., 2005), and nanoscale interactions between quartz and water (Pope, 1995). The new generation of higher resolution BSE detectors is able to generate nanoscale resolution to illustrate both internal and external modes of quartz silt production (**Fig. 26**).

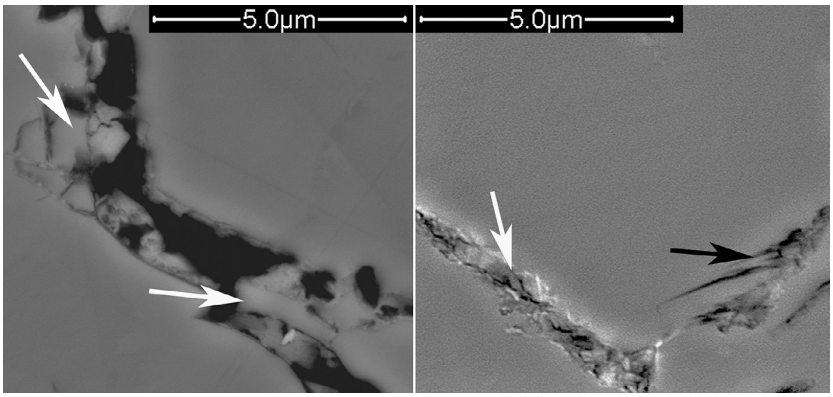

Fig. 26 Images of quartz weathering observed in a desert pavement near Florence Junction, Arizona. These images show formation of silt-sized quartz fragments that appear to depend on both the existence of a fracture inside the quartz grain (white arrows) and also fragmenting along angles that are not aligned with the fracture (black arrows). For example, the subparallel fracturing seen in the right image likely relates to aligned crystal defects. However, the jig-saw puzzle appearance of quartz fragments on the edge of the fracture (upper left white arrow) in the left image is not easily explained by aligned defects.

The transition between wind-transported dust and dust as an integrated component of rock coatings has seen surprisingly little study. Even though there is a general consensus in the rock coating literature that aeolian dust contributes to the formation of rock varnish, phosphate skins, and silica glaze (Dorn, 1998, 2009; Langworthy et al., 2010; Potter and Rossman, 1977), we do not know of a systematic study of nanoscale alternations of dust in the transition from rock-surface loess to rock coating constituent.

We present here a nanoscale study of the transition from dust to rock coating in the Ashikule Basin, Tibet (**Fig. 27**). The 4700—4800 m high graben is a dusty, sulfate-rich, high-elevation and high UV flux environment. This field site offers the opportunity to study dust/substrate interactions distant from industrial pollution. The cold, dry, lower-air pressure nature of the field suggests potential for a Mars analog site in part because the substrate is a lava flow, a trachyandesite of Ashishan Volcano in the Akesu Volcanic field (Wei et al., 2003).

While nanoscale mineral etching is of key importance as a process in chemical weathering, etched mineral surfaces could also play a role in the initial stages of the physical attachment of dust particles to mineral surfaces. Dust accretion on mineral surfaces is generally thought to occur from electrostatic or physical forces that hold dust particles together (Bishop et al., 2002; Ganor et al., 2009; Jordan, 1954). Nanoscale mineral etching creates an irregular surface that could play a key role in the initial attraction (**Fig. 28**).

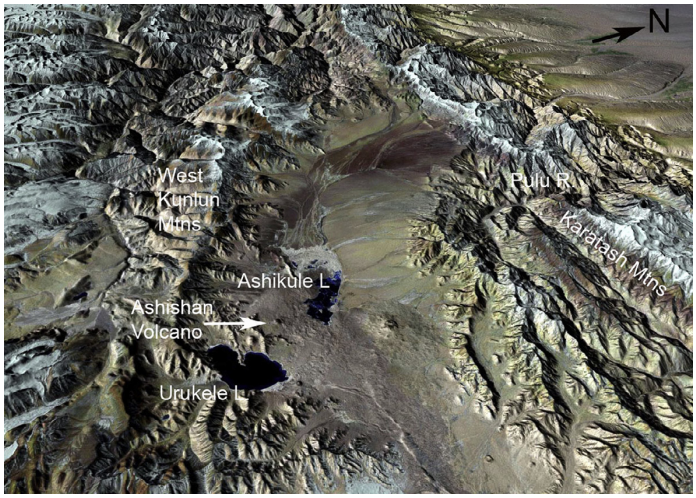

Fig. 27 Ashishan Volcano study site in the Ashikule Basin, Tibet at 35.6988°N, 81.57623°E. The length of Urukele Lake is about 7 km, Ashikule Lake about 5.5 km, and the width of the graben at the location of the Ashishan Volcano is about 22 km. Modified from a raw image designed by William Bowen.

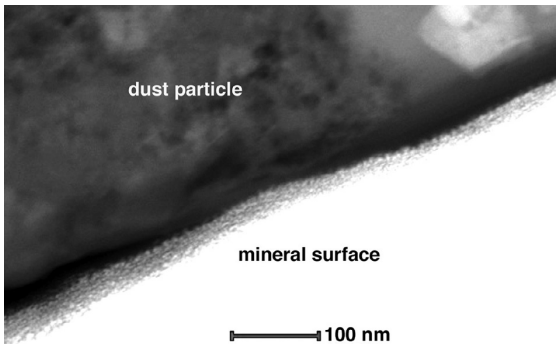

Fig. 28 Mineral etching creates nanotopographic irregularities on the scale of less than 10 nm, as seen in this HRTEM image of cross-section of a dust particle attracted to the underlying mineral surface of a rock. Nanoscale topographic irregularities likely contributed to the physical attachment of dust to this mineral surface, collected from the Akesu volcanic field, Tibet.

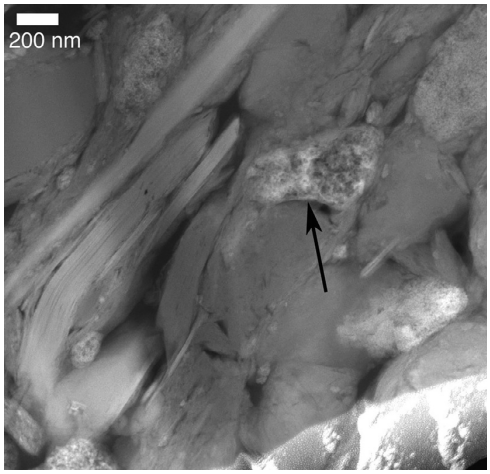

Fig. 29 HRTEM image of dust particles on top of silica glaze and rock varnish. Many dust particles appear to be clay minerals, while others are fragments of other minerals. We selected a particle with two oval forms that could have a biotic origin (arrow). These oval forms appear to be undergoing post-depositional modification, as indicated by the uneven texture of bright and dark areas that suggest differential movement of elements.

The particular sample selected for a detailed elemental nanoscale analysis is dust that accumulated on top of a rock coating that is a mixture of silica glaze and rock varnish. Silica glaze dominates this rock coating, but pods of rock varnish 2–40 μm across exist and are enveloped by the silica glaze (Krinsley et al., 2009; Langworthy et al., 2010). We selected a form with two oval shapes in the dust on top of the rock coating. This pod-form has a texture suggestive of a biological origin (**Fig. 29**), in that it has a granular texture similar to microbial hyphae observed elsewhere (Bonneville et al., 2009).

Our nanoscale investigation of grain alternation generated EDX data in a pattern of 300 points in a 10×30 matrix, where measurements are taken approximately 1.3 nm apart. Beam damage allows visualization (Lee, 2010) of the clear grid pattern (**Fig. 30**). The grid serves as ground control points, allowing mapping of digital EDX data with geographic information system (GIS) software and subsequent visualization of nanoscale weathering.

Fig. 31 displays a visualization of the 300-point grid of EDX data using a Kriging algorithm to map out elemental patterns. The dominant peaks in the EDX analyses consisted of the inorganic components of silicon and oxygen, and potential organic components of carbon and phosphorus. The highest concentrations of Si and O occur underneath the granular oval; this particle has a parallel structure suggestive of a clay mineral composition that would be consistent with the higher abundance of Si and O. In contrast, the highest concentration of carbon occurs where the oval form displays a gray granular texture that transitions to an area of greater porosity with the lowest carbon concentrations. The area richest in C does appear to correspond with high P concentrations, but some areas of high P do have low concentrations of C. Banfield et al. (1999: 3407) found potential complex mixtures of clay minerals and complex organic polymers associated with microbial weathering, and this is a possible for the analyzed oval in **Figs. 30 and 31**.

Visualization of nanoscale spatial geochemistry with EDX grids has been accomplished in mineralogical research (Lee, 2010), but not analyzing rock coatings. Thus, the following interpretation of this single pilot analysis is speculative. Starting with the

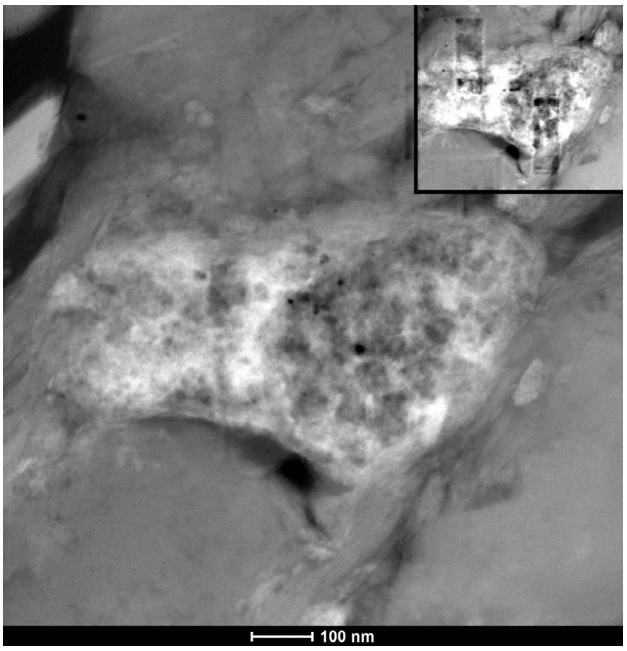

Fig. 30 EDX data were collected in a grid pattern, where X-rays were generated every 1.3 nm apart. The center right part of the particle appears to be the most porous. The beam damage (seen in upper right inset image) creates a grid on the sample, and thus the precise locations of data are known and can be analyzed using geostatistical methods.

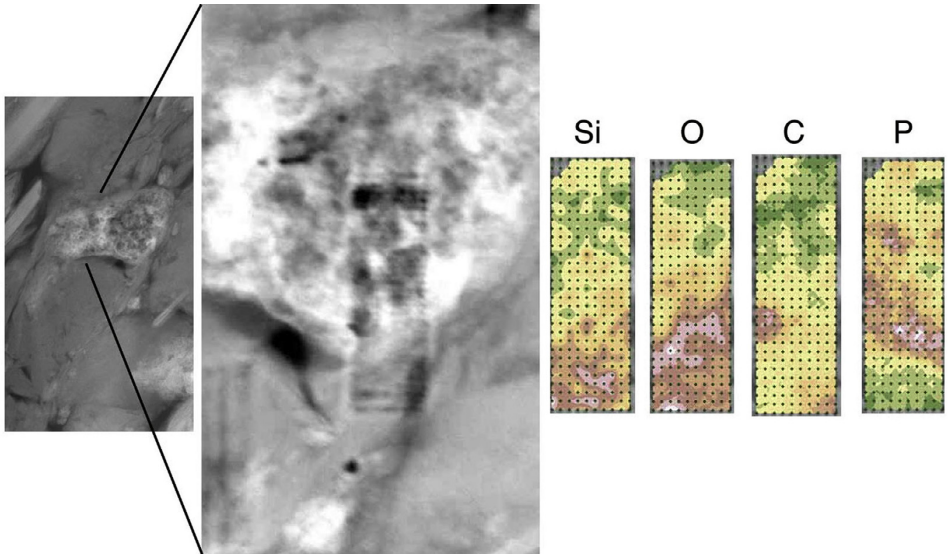

Fig. 31 Nanoscale EDX mapping of a 300-point grid. Each grid point is approximately 1.3 nm apart, and the grid is 10 columns and 30 rows. The visual grid corresponds in size with maps of the four most common elements. **Fig. 30** shows the larger context and a HRTEM pre-beam-damaged image of the analyzed area. The Kriging algorithm used to map out elemental patterns presents an intuitive color scale where lowest values are dark green and highest values are brown to pink.

assumption that the oval particle had an organic origin, it appears as though Si and O (likely silica) has begun to migrate from the underlying clay inward—a possibility deduced by the gradient of Si and O from the clay at the bottom into the granular particle. The lower levels of C at the top of the grid could reflect the electron transparency of the middle of the oval form; picture sectioning a highly desiccated bacterial cell (or cross-section of a desiccated fungal hypha). The thickest portions would be on the margins,

while the center would be thinnest—explaining why the lowest carbon concentrations occur in the middle of a possible desiccated microbial form. The behavior of phosphorus appears to link with a brighter area of the HRTEM image, and this bright area sends stringers toward the upper left. Like Si and O, the spatial pattern of phosphorus suggests nanoscale movement and hence instability. Our interpretation of nanoscale instability is not unique to rock coatings such as rock varnish (Dorn, 1998; Dorn and Krinsley, 2019; Krinsley, 1998; McKeown and Post, 2001) or silica glaze (Dorn, 1998; Gordon and Dorn, 2005b; Langworthy et al., 2010). However, it appears as though nanoscale movement of inorganic and possible organic components starts in dust deposits on rock surfaces—prior to envelopment inside a rock coating.

3.09.7 From nanoscale to landscape scale: Applications of meteoric ^{10}Be and ^{10}Be/^{9}Be to the study of Earth's surface

Meteoric ^{10}Be is a cosmogenic radionuclide with a half-life ($t_{1/2}$) of 1.39 million years (Chmeleff et al., 2010; Korschinek et al., 2010). Cosmogenic ^{10}Be produced within minerals is very different in that it builds up within minerals like quartz. Also, the concentration of *in situ* produced ^{10}Be is negligible compared to much greater meteoric ^{10}Be concentrations. Meteoric ^{10}Be is more like ^{14}C that is produced within the atmosphere by nuclear reactions and delivered by snow, rain or by dry deposition to Earth's surfaces (Fig. 32A). Unlike radiocarbon that is best dated in association with preserved organic matter (e.g., tree wood), meteoric ^{10}Be

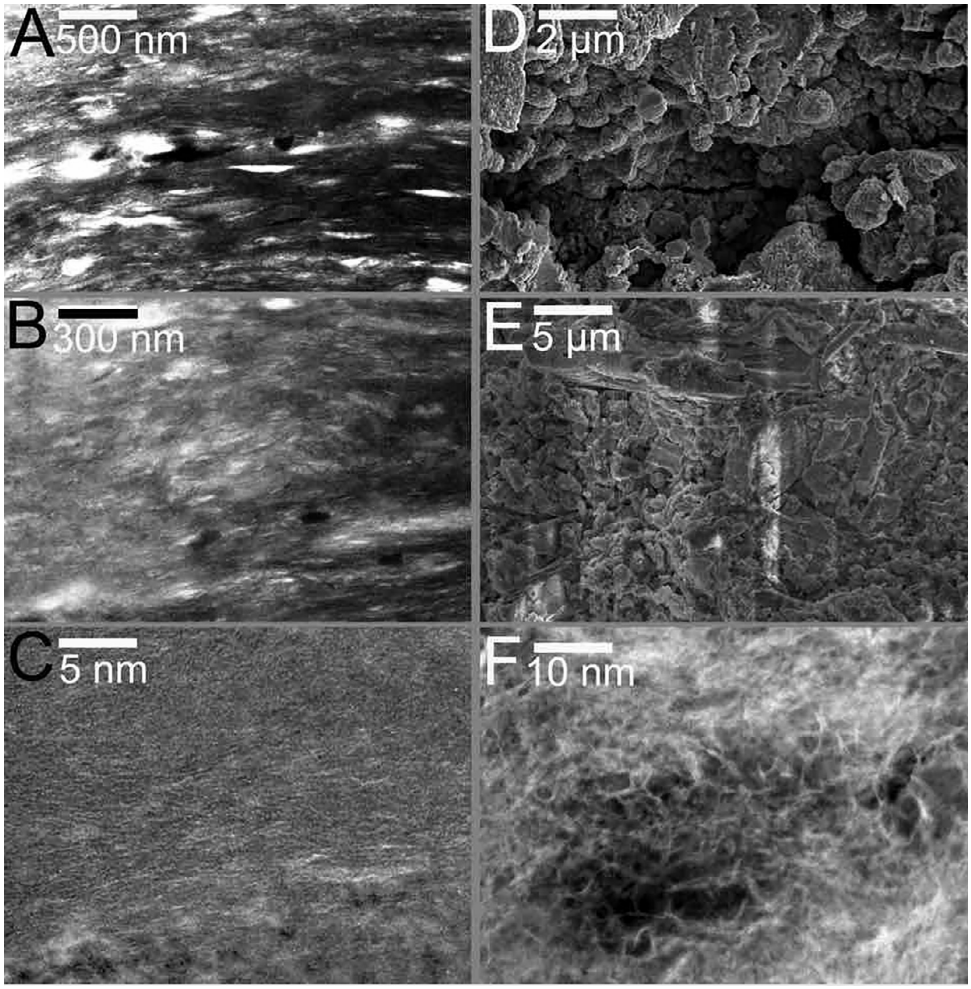

Fig. 32 Nanoscale textures of Lake Bidahouchi lacustrine sediment offer insight into distinguishing closed-system and open-system deposits for meteoric ^{10}Be and authigenic ^{10}Be/^{9}Be dating. (A–C) laminar textures at course and fine nanoscales produce statistically similar results for dating. (D–F) irregular and non-laminar textures are associated with inconsistent ^{10}Be/^{9}Be ratios.

that rains out of the atmosphere rapidly adsorbs to soil or river, lacustrine, and marine sediment particles (Willenbring and von Blanckenburg, 2010).

Geomorphologists have been struggling to determine how best to use meteoric ^{10}Be that is strongly adsorbed to smaller particles at pH > 6 (Willenbring and von Blanckenburg, 2010; You et al., 1989). A key strategy is comparing ^{10}Be with the stable isotope ^{9}Be to circumvent an issue associated with grain size dependency and retentivity (von Blanckenburg et al., 2012). One way that geomorphologists have used this cosmogenic nuclide is to study seafloor deposits underneath ice shelves or ice sheets (Yokoyama et al., 2016; White et al., 2019) that impede the delivery of meteoric ^{10}Be to the seafloor providing a proxy for ice sheet retreat (Jeong et al., 2018).

Meteoric ^{10}Be and authigenic ^{10}Be/^{9}Be ratios can provide a powerful tool for dating lacustrine, marine sediment and floodplain deposits (Bourlès et al., 1989; Seong et al., 2016). Age calculations are performed as follows:

$$t = -(1/\lambda) \times \ln\left(N_{(t)}/N_0\right) \text{ or } t = -(1/\lambda) \times \ln\left(R_{(t)}/R_0\right)$$

where λ is decay constant ($ln(2)/t_{1/2} = 5 \times 10^{7}$ year^{-1}) of ^{10}Be, $N_{(t)}$ [atoms g^{-1}] is the meteoric ^{10}Be concentration measured in the sample, N_0 is the initial meteoric ^{10}Be concentration, $R_{(t)}$ is the measured authigenic ^{10}Be/^{9}Be, and R_0 is the initial authigenic ^{10}Be/^{9}Be.

There are two prerequisites for applying ^{10}Be/^{9}Be for the age calculations (Lebatard et al., 2010; Šujan et al., 2016): (1) the initial authigenic ^{10}Be/^{9}Be (R_0) should be accurately determined, (2) the samples should have remained in closed system which means that any beryllium isotopes should not enter or escape the sample after deposition. Globally, R_0 in ocean deposits have been relatively constant over the last 12 Ma (Willenbring and von Blanckenburg, 2010), and locally it was confirmed that the R_0 remains stable in large continental basins like Lake Chad (Lebatard et al., 2010) and in the northern Danube Basin (Šujan et al., 2016) over the last 8 and 11 Ma, respectively. The R_0 should always be measured in recent samples deposited in similar environmental settings (Lebatard et al., 2010), because meteoric ^{10}Be flux is dependent on latitudes (Masarik and Beer, 2009) and ^{9}Be inputs are depending on the geological composition of the drainage basin and on sedimentary environments (Šujan et al., 2016).

The second prerequisite of a closed system (or approximating a closed system) is where nanoscale weathering processes become important. As a dating method, the authigenic ^{10}Be/^{9}Be particularly useful when biostratigraphical data is scarce due to the interaction of complex processes (lacustrine, deltaic and alluvial) to deposit and supported by limited geochronological data with only a few grams of fine grained sediment (Šujan et al., 2016). Authigenic ^{10}Be/^{9}Be is also very useful because it can be used to date sediments that include the Quaternary and Pliocene.

The deposits of an ancient lake could hold the key to the origin of the Grand Canyon of the Colorado River, southwestern USA, provide an example of the importance of nanoscale processes. Meek and Douglass (2001) hypothesized that overflow of Lake Bidahouchi led to the formation of the Grand Canyon. Although this hypothesis is consistent with available geomorphic criteria (Douglass et al., 2009), confirming or disconfirming evidence has been difficult to obtain including the age of Lake Bidahouchi's youngest deposits. Douglass et al. (2020) used ^{87}Sr/^{86}Sr to document that these youngest preserved deposits have a Colorado River signal. Douglass et al. (2020) also compared Bidahouchi ^{10}Be/^{9}Be to Bouse Formation (lacustrine) deposits along the lower Colorado River (Pearthree and House, 2014). For the lake overflow hypothesis to be possible, the youngest Lake Bidahouchi deposits must slightly post-date the youngest lacustrine deposits far downstream (Bouse Formation). The hypothesis is that Bidahouchi overflowed to initiate Grand Canyon incision, and this then led to a through-flowing Colorado River that then breached closed basin lakes (cf. Bouse Formation) downstream.

Thus, Bidahouchi and Bouse lacustrine deposits were evaluated for ^{10}Be/^{9}Be, with reasonable assumption that the production rate in this same region and in same general timeframe of the late Pliocene would have been the same. While the Bouse deposits had a ^{10}Be/^{9}Be ratio consistent with the cessation of deposition ca. 5 Ma, the Lake Bidahouchi youngest deposits had mixed ^{10}Be/^{9}Be results (Douglass et al., 2020). One group of Lake Bidahouchi deposits had ^{10}Be/^{9}Be ratios with a tight cluster that is slightly older than the Bouse deposits, consistent with the idea of lake overflow leading to Grand Canyon's formation. Another group of Lake Bidahouchi deposits had variable ^{10}Be/^{9}Be ratios.

A nanoscale analysis reveals why. Fine grained Lake Bidahouchi deposits with minimal internal porosity at the nanoscale (e.g., **Fig. 32**A–C) provide a closed system for the beryllium. In contrast, Lake Bidahouchi deposits with textures more susceptible to diagenesis (**Fig. 32**D–F) increase the ability of groundwater to move through the sediment and mobilize beryllium taking it out of a closed system. Without this sort of nanoscale insight, it would not be possible to distinguish open from closed Lake Bidahouchi sediment.

3.09.8 Conclusion

Rock decay (weathering) is a multidisciplinary arena explored by geochemists, soil scientists, geomorphologists, hydrologists, civil and environmental engineers, archaeologists, planetary geologists, and others interested in the breakdown and decay of rocks. Geomorphologists were among the first to explore the importance of nanoscale processes in rock decay (Eggleton, 1980; Krinsley et al., 1995; Pope, 1995), even though nanoscale research in weathering has been dominated by geochemists over the past two

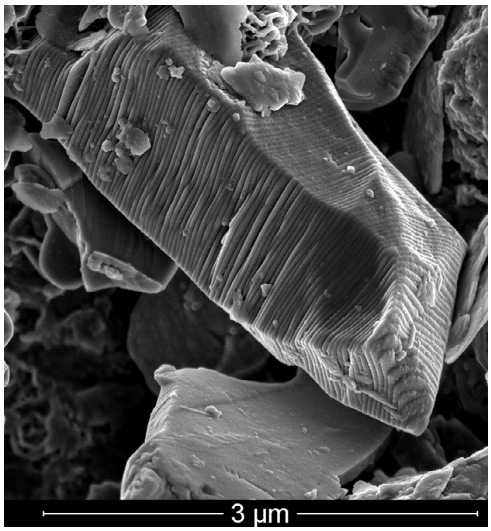

Fig. 33 Decay of biotite mineral, Adirondack Mountains, New York. The subparallel fracturing called splintering is a result of weathering that is taking place at the nanoscale.

decades (Banfield and Eggleton, 1988; Banfield et al., 1999; Hochella, 2002a; Hochella et al., 2008; Waychunas et al., 2005). A consequence of a general lack of attention to the nanoscale by geomorphologists has resulted in situation where few connections exist between Earth's landforms and the nanoscale.

Certainly, rock decay theory in geomorphology is concerned with scale (Hall, 2006b; Phillips, 2000; Pope et al., 1995; Viles, 2001; Turkington et al., 2005). However, the "microscale" in geomorphic theory has been the subject of research at micrometer and more extensive areas. Nanoscale processes operating between one nanometer (10^{-9} m) and 100 nm (10^{-7} m) or 0.1 µm (**Fig. 1**) do not reflect microscale conditions or processes.

Physical, electrical, magnetic, thermal, and kinetic properties differ dramatically across the nano-micron threshold (Hochella, 2002b; Zhang et al., 2003). The behavior of water in microfractures supporting capillary flow at the micron scale (Dorn, 2003; Dixon and Thorn, 2005; Meunier et al., 2007) does not reflect the behavior of nanoscale water (Kalinichev et al., 2007; Langworthy et al., 2010; Lower et al., 2001; Wang et al., 2006; Zhang et al., 2003). An example comes from brucite, a magnesium hydroxide that is a common weathering product (Kalinichev et al., 2007). Kalinichev et al. (2007) modeled three well-defined layers with respect to the behavior of water within 15 angstroms of a brucite surface. There is an inner layer of a few angstroms that is highly structured and contains water molecules with a high atomic density coordinated to the brucite surface. There is a middle transition layer about four angstroms from the surface with a low atomic density, and the outer layer that becomes similar to bulk nanoscale water about 5–15 Å from the surface. A similar result comes from studies of how water adheres to mica (Xu et al., 2010), where the first and second 0.4 nm layers of water behaves like ice and accumulates at surface defects, but thicker accumulations of water are liquid-like.

A large realm of considerable challenge in nanoscale weathering research rests in explaining weathering forms such as those displayed in **Fig. 33**. A biotite grain that is undergoing splintering has split into subparallel fragments as a result of nanoscale weathering processes by water accumulating at surface defects. The next generation of weathering researchers will link nanoprocesses to such micron-scale forms with such technology as coupled dual-beam focused ion beam electron microscopy (FIB-EM) (**Table 1**).

Linking nano- and micron-scales will involve exceptionally different and hard-to-predict behavior such as biologically generated particles. In many cases, nanobiominerals are more stable (Tang et al., 2004) than would be expected of inorganic counterparts. In other cases, they are less stable (Dorn, 1998; Krinsley, 1998) than inorganic counterparts, for reasons. Given the dominance of microorganisms on Earth (Reith, 2011), biologically generated particles will be a persistant issue in all aspects of nanoscale weathering.

Further development of theory as it applies to understanding rock decay forms needs to cross the nano-micron threshold. Unfortunately, very little research exists connecting nanoscale processes and geomorphic forms. For example, Hall (2006a: 388) argued that "little or no recognition has been given to either the processes or the measuring of attributes influencing the [freeze-thaw] processes or the measuring of attributes influencing the weathering processes, at the micro-scale, let alone the nano-scale." Until nanoscale observations are woven into the fabric of understanding such basic processes as frost weathering, it would be premature to develop geomorphic theory further. We do not believe that there exists a sufficient understanding to be able to link the nano-micron threshold with a new theoretical understanding of landforms. Instead, this article represents an attempt to provide empirical case studies exemplifying why nanoscale matters to geomorphology.

Acknowledgments

We thank reviewers and Greg Pope, the volume editor, for their suggestions. We gratefully acknowledge the help and vision of the late Dr. David Krinsley, and of Kurt Langworthy, who as our co-authors in the 2011 article had a profound impact on our understanding of the nanoscale. We also acknowledge Dr. Yeong Bae Seong for his help in vision in understanding the importance of cosmmogenic nuclides in understanding earth-surface processes.

References

Ahnert, F., 1976. Brief discription of a comprehensive three-dimensional process-response model of landform development. Zeitschrift fur Geomorphologie Supplementband 25, 29–49.

Balogh-Brunstad, Z., Smart, K., Dohnalkova, A., Saccone, L., Smits, M.M., 2020. Micro- and nanoscale techniques to explore bacteria and fungi interactions with silicate minerals. In: Dontsova, K., Balogh-Brunstad, Z., Le Roux, G. (Eds.), Biogeochemical cycles, ecological drivers, and environmental impact. American Geophysical Union, Washington D.C. https://doi.org/10.1002/9781119413332.ch4.

Banfield, J.F., Barker, W.W., 1994. Direct observation of reactant-product interfaces formed in natural weathering of exsolved, defective amphibole to smectite: Evidence for episodic, isovolumetric reactions involving structural inheritance. Geochimica Cosmochimica Acta 58, 1419–1429.

Banfield, J.F., Eggleton, R.A., 1988. Transmission electron microscopy study of biotite weathering. Clays and Clay Minerals 36, 47–60.

Banfield, J.F., Eggleton, R.A., 1990. Analytical transmission electron microscope studies of plagioclase, muscovite and K-feldsapr weathering. Clay and Clay Minerals 38, 77–89.

Banfield, J.F., Barker, W.W., Welch, S.A., Taunton, A., 1999. Biological impact on mineral dissolution: Application of the lichen model to understanding mineral weathering in the rhizosphere. Proceedings of the National Academy of Sciences of the United States of America 96, 3404–3411.

Barker, W.W., Banfield, J.F., 1996. Biologically versus inorganically mediated weathering reactions: Relationships between minerals and extracellular microbial polymers in lithobiontic communities. Chemical Geology 132, 55–69.

Basile-Doelsch, I., Balesdent, J., Rose, J., 2015. Are interactions between organic compounds and nanoscale weathering minerals the key drivers of carbon storage in soils? Environmental Science & Technology 49, 3997–3998.

Bennett, P.C., Rogers, J.R., Choi, W.J., Hiebert, F.K., 2001. Silicates, silicate weathering, and microbial ecology. Geomicrobiology Journal 18, 3–19.

Benzerara, K., Menguy, N., Guyot, F., Vanni, C., Gillet, P., 2005a. TEM study of a silicate-carbonate-microbe interface prepared by focused ion beam milling. Geochimica Cosmochimica Acta 69, 1413–1422.

Benzerara, K., Yoon, T.H., Menguy, N., Tyliszczak, T., Brown, G.E., 2005b. Nanoscale environments associated with bioweathering of a Mg-Fe-pyroxene. Proceedings of the National Academy of Sciences of the United States of America 102, 979–982.

Bishop, J.L., Murchie, S.L., Pieters, C.M., Zent, A.P., 2002. A model for formation of dust, soil, and rock coatings on Mars: Physical and chemical processes on the Martian surface. Journal of Geophysical Research 107 (E11). https://doi.org/10.1029/2001JE001581.

Bjelland, T., Thorseth, I.H., 2002. Comparative studies of the lichen-rock interface of four lichens in Vingen, western Norway. Chemical Geology 192, 81–98.

Bonneville, S., Smits, M.M., Brown, A., Harrington, J., Leake, J.R., Brydson, R., Benning, L.G., 2009. Plant-driven fungal weathering: Early stages of mineral alteration at the nanometer scale. Geology 37, 615–618.

Bourlès, D., Raisbeck, G.M., Yiou, F., 1989. 10Be and 9Be in marine sediments and their potential for dating. Geochimica et Cosmochimica Acta 53, 443–452.

Brady, P.V., 1991. The effect of silicate weathering on global temperature and atmospheric CO_2. Journal of Geophysical Research 96 (B), 18101–18106.

Brady, P.V., Dorn, R.I., Brazel, A.J., Clark, J., Moore, R.B., Glidewell, T., 1999. Direct measurement of the combined effects of lichen, rainfall, and temperature on silicate weathering. Geochimica et Cosmochimica Acta 63, 3293–3300.

Brandt, F., Bosbach, D., Krawczyk-Barsch, E., Arnold, T., Bernhard, G., 2003. Chlorite dissolution the acid pH-range: A combined microscopic and macroscopic approach. Geochimica et Cosmochimica Acta 67, 1451–1462.

Brantley, S.L., 2005. Reaction kinetics of primary rock-forming minerals under ambient conditions. In: Drever, J.I. (Ed.), Surface and ground water, weathering, and soils. Treastise on geochemistry, vol. 5. Elsevier, Amsterdam, pp. 73–117.

Brantley, S.L., Mellott, N.P., 2000. Surface area and porosity of primary silicate minerals. American Mineralogist 85, 1767–1783.

Brantley, S.L., Velbel, M.A., 1993. Preface to special issue on geochemical kinetics of mineral-water reactions in the field and the laboratory. Chemical Geology 105, vii–ix.

Brantley, S.L., Eissenstat, D.M., Marshall, J.A., Godsey, S.E., Balogh-Brunstad, Z., Karwan, D.L., Papuga, S.A., Roering, J., Dawson, T.E., Evaristo, J., Chadwick, O., 2017. Reviews and syntheses: On the roles trees play in building and plumbing the critical zone. Biogeosciences 14, 5115–5142.

Brehm, U., Gorbushina, A.A., Mottershead, D.N., 2005. The role of microorganisms and biofilms in the breakdown and dissolution of quartz and glass. Palaeogeography, Palaeoclimatology, Palaeoecology 219, 117–129.

Brown, D.J., Lee, M.R., 2007. From microscopic minerals to global climate change? Geology Today 23 (5), 172–177.

Bullard, J.E., Livingston, I., 2009. Dust. In: Parsons, A.J., Abrahams, A.D. (Eds.), Geomorphology of Desert Environments. Springer, New Work, pp. 629–654.

Buss, H.L., Lüttge, A., Brantley, S.L., 2007. Etch pit formation on iron silicate surfaces during sideophore-promoted dissolution. Chemical Geology 240, 326–342.

Campbell, S.W., 1999. Chemical weathering associated with tafoni at Papago Park, Central Arizona. Earth Surface Processes and Landforms 24, 271–278.

Campbell, E.M., Twidale, C.R., 1991. The evolution of bornhardts in silicic volcanic rocks in the Gawler ranges. Australian Journal of Earth Sciences 38, 79–93.

Campbell, S.W., Dixon, J.C., Darmody, R.G., Thorn, C.E., 2001. Spatial variation of early season surface water chemistry in Karkevagge, Swedish Lapland. Geografiska Annaler A 83A, 169–178.

Campbell, S.W., Dixon, J.C., Thorn, C.E., Darmody, R.G., 2002. Chemical denudation rates in Karkevagge, Swedish Lapland. Geografiska Annaler A 84A, 179–185.

Casey, W.H., Banfield, J.F., Westrich, H.R., McLaughlin, L., 1993. What do dissolution experiments tell us about natural weathering? Chemical Geology 105, 1–15.

Certini, G., Corti, G., Ugolini, F.C., DeSiena, C., 2002. Rock weathering promoted by embryonic soils in surface cavities. European Journal of Soil Science 53, 139–146.

Chitale, J.D., 1986. Study of petrography and internal structures in calcretes of West Texas and New Mexico (Microtextures, Caliche). Ph.D. Dissertation [Thesis thesis]. Texas Tech University, Lubbock.

Chmeleff, J., von Blanckenburg, F., Kossert, K., Jakob, D., 2010. Determination of the 10Be half-life by multicollector ICP-MS and liquid scintillation counting. Nuclear Instruments and Methods in Physics Research Section B Beam Interactions With Material and Atoms 268, 192–199.

Churaev, N.V., 2003. Surface forces in wetting films. Advances in Colloid and Interface Science 103, 197–218.

Conca, J.L., Rossman, G.R., 1982. Case hardening of sandstone. Geology 10, 520–525.

Coudé-Gaussen, G., Rognon, P., Federoff, N., 1984. Piegeage de poussières éoliennes dans des fissures de granitoides due Sinai oriental. Compte Rendus de l'Academie des Sciences de Paris II 369–374.

Darmody, R.G., Thorn, C.E., Dixon, J.C., 2008. Differential rock weathering in the 'Valley of the Boulders', Karkevagge Swedish Lapland. Geografiska Annaler A 90A, 201–209.

Dixon, J.C., 1986. Solute movement on hillslopes in the alpine environment of the Colorado Front Range. In: Abrahams, A.D. (Ed.), Hillslope processes. Allen and Unwin, London, pp. 139–159.

Dixon, J.C., 2013. Chemical weathering in cold climates. In: Pope, G. (Ed.), Treatise on geomorphology, 4. Academic Press, San Diego, pp. 245–257.

Dixon, J.C., 2018. Stone pavements, lag deposits, and contemporary landscape evolution. In: Soare, R.J., Conway, S.J., Clifford, S.M. (Eds.), Dynamic Mars: Recent and current evolution of the red planet. Elsevier, Amsterdam, pp. 387–410.
Dixon, J.C., Thorn, C.E., 2005. Chemical weathering and landscape development in alpine environments. Geomorphology 67, 127–145.
Dixon, J.C., Thorn, C.E., Darmody, R.G., 1984. Chemical weathering processes on the Vantage Peak nunatak, Juneau Icefield, southern Alaska. Physical Geography 5, 111–131.
Dixon, J.C., Thorn, C.E., Darmody, R.G., Campbell, S.W., 2002. Weathering rinds and rock coatings from an Arctic alpine environment, northern Scandinavia. Geological Society of America Bulletin 114, 226–238.
Dorn, R.I., 1995. Digital processing of back-scatter electron imagery: A microscopic approach to quantifying chemical weathering. Geological Society of America Bulletin 107, 725–741.
Dorn, R.I., 1998. Rock coatings. Elsevier, Amsterdam, 429 p.
Dorn, R.I., 2003. Boulder weathering and erosion associated with a wildfire, Sierra Ancha Mountains, Arizona. Geomorphology 55, 155–171.
Dorn, R.I., 2004. Case hardening. In: Goudie, A.S. (Ed.), Encyclopedia of geomorphology. Routledge, London, pp. 118–119.
Dorn, R.I., 2007. Rock varnish. In: Nash, D.J., McLaren, S.J. (Eds.), Geochemical sediments and landscapes. Blackwell, London, pp. 246–297.
Dorn, R.I., 2009. Desert rock coatings. In: Parsons, A.J., Abrahams, A. (Eds.), Geomorphology of desert environments. Springer, Amsterdam, pp. 153–186.
Dorn, R.I., 2011. Revisiting dirt cracking as a physical weathering process in warm deserts. Geomorphology 135, 129–142.
Dorn, R.I., 2014. Ants as a powerful biotic agent of olivine and plagioclase dissolution. Geology 42, 771–774.
Dorn, R.I., 2016. Identification of debris-flow hazards in warm deserts through analyzing past occurrences: Case study in South Mountain, Sonoran Desert, USA. Geomorphology 273, 269–279.
Dorn, R.I., 2018. Necrogeomorphology and the life expectancy of desert bedrock landforms. Progress in Physical Geography 82, 566–587.
Dorn, R.I., Brady, P.V., 1995. Rock-based measurement of temperature-dependent plagioclase weathering. Geochimica et Cosmochimica Acta 59, 2847–2852.
Dorn, R.I., Krinsley, D., 2019. Nanoscale observations support the importance of chemical processes in rock decay and rock coating development in cold climates. Geosciences Journal 9. https://doi.org/10.3390/geosciences9030121.
Dorn, R.I., Whitley, D.S., Cerveny, N.C., Gordon, S.J., Allen, C., Gutbrod, E., 2008. The rock art stability index: A new strategy for maximizing the sustainability of rock art as a heritage resource. Heritage Management 1, 35–70.
Dorn, R.I., Dorn, J., Harrison, E., Gutbrod, E., Gibson, S., Larson, P., Cerveny, N., Lopat, N., Groom, K.M., Allen, C.D., 2012. Case hardening vignettes from the western USA: Convergence of form as a result of divergent hardening processes. Association of Pacific Coast Geographers Yearbook 74, 1–12.
Dorn, R.I., Mahaney, W.C., Krinsley, D.H., 2017. Case hardening: Turning weathering rinds into protective shells. Elements 13, 155–158.
Douglass, J., Meek, N., Dorn, R.I., Schmeeckle, M.W., 2009. A criteria-based methodology for determining the mechanism of transverse drainage development, with application to the southwestern United States. Geological Society of America Bulletin 121, 586–598.
Douglass, J., Gootee, B.F., Jeong, A., Seong, Y.B., 2020. The overflow origin of the Grand Canyon. Geomorphology 369. https://doi.org/10.1016/j.geomorph.2020.107361.
Eggleton, R.A., 1980. High resolution electron microscopy of feldspar weathering. Clays and Clay Minerals 28, 173–178.
Ehlen, J., 2002. Some effects of weathering on joints in granitic rocks. Catena 91–109.
Emmanuel, S., 2014. Mechanisms influencing micron and nanometer-scale reaction rate patterns during dolostone dissolution. Chemical Geology 363, 262–269.
Engelder, T., 1987. Joints and shear fractures in rock. In: Atkinson, B. (Ed.), Fracture mechanics of rock. Academic Press, Orlando, pp. 27–69.
Eyles, N., Arnaud, E., Scheidegger, A.E., Eyles, C.H., 1997. Bedrock jointing and geomorphology in southwestern Ontario, Canada: An example of tectonic predesign. Geomorphology 19, 17–34.
Finlay, R.D., Mahmood, S., Rosenstock, N., Bolou-Bi, E.B., Köhler, S.J., Fahad, Z., Rosling, A., Wallander, H., Belyazid, S., Bishop, K., Lian, B., 2020. Biological weathering and its consequences at different spatial levels–from nanoscale to global scale. Biogeosciences Discussions 17, 1507–1533.
Fitzner, B., Heinrichs, K., 2004. Photo atlas of weathering forms on stone monuments. http://www.stone.rwth-aachen.de/. Accessed 7/18/2010.
Fitzner, B., Heinrichs, K., Kownatski, R., 1997. Weathering forms at natural stone monuments - classification, mapping and evaluation. International Journal for Restoration of Buildings and Monuments 3 (2), 105–124.
Frazier, C.S., Graham, R.C., 2000. Pedogenic transformation of fractured granitic bedrock, southern California. Soil Science Society of America Journal 64, 2057–2069.
Gadd, G.M., 2007. Geomycrology: Biogeochemical transformations of rocks, minerals, metals and radionuclides by fungi, bioweathering and bioremediation. Mycological research 111, 3–49.
Gadd, G.M., 2017. Fungi, rocks, and minerals. Elements 13, 171–176.
Gaier, J.R., 2005. The effects of lunar dust on EVA systems during the Apollo missions. In: NASA/TM—2005-213610. NASA Center for Aerospace Information, Hanover, Maryland, 66 p.
Ganor, E., Kronfeld, J., Feldman, H.R., Rosenfeld, A., Ilani, S., 2009. Environmental dust: A tool to study the patina of ancient artifacts. Journal of Arid Environments 73, 1170–1176.
Garvie, L.A.J., Burt, D.M., Buseck, P.R., 2008. Nanometer-scale complexity, growth, and diagenesis in desert varnish. Geology 36, 215–218.
Garvie, L.A.J., Burt, D.M., Buseck, P.R., 2009. A microscopists view of desert varnish from the Sonoran Desert. In: Lunar and Planetary Science Conference 40, 1344.pdf.
Gilbert, G.K., 1877. Geology of the Henry Mountains. U.S. Geological and Geographical Survey, Washington D.C., 160 p.
Gleeson, D.B., Clipson, N., Melville, K., Gadd, G.M., McDermott, F.P., 2005. Characterization of fungal community structure on a weathered pegmatitic granite. Microbial Ecology 50, 360–368.
Gleeson, D.B., Kennedy, N.M., Clipson, N., Melville, K., Gadd, G.M., McDermott, F.P., 2006. Characterization of bacterial community structure on a weathered pegmatitic granite. Microbial Ecology 51, 526–534.
Goldich, S.S., 1938. A study of rock weathering. Journal of Geology 46, 17–58.
Gordon, S.J., Brady, P.V., 2002. In situ determination of long-term basaltic glass dissolution in the unsaturated zone. Chemical Geology 90, 115–124.
Gordon, S.J., Dorn, R.I., 2005a. In situ weathering rind erosion. Geomorphology 67, 97–113.
Gordon, S.J., Dorn, R.I., 2005b. Localized weathering: Implications for theoretical and applied studies. Professional Geographer 57, 28–43.
Goudie, A.S., 1978. Dust storms and their geomorphological implications. Journal of Arid Environments 1, 291–310.
Hall, K., 1993. Enhanced bedrock weathering in association with late-lying snowpaches: Evidence from Livingston Island, Antarctica. Earth Surface Processes and Landforms 18, 121–129.
Hall, K., 1999. The role of thermal stress fatigue in the breakdown of rock in cold regions. Geomorphology 31, 47–63.
Hall, K., 2006a. Monitoring of thermal conditions in building stone with particular reference to freeze-thaw events. In: Kourkoulis, S.K. (Ed.), Fracture and failture of natural building stones. Springer, Amsterdam, pp. 373–394.
Hall, K., 2006b. Perceptions of rock weathering in cold regions: A discussion on space and time attributes of scale. Géomorphologie: Relief, Processus, Environnement 3, 187–196.
Hall, K., André, M.F., 2001. New insights into rock weathering from high-frequency rock temperature data: An Antarctic study of weathering by thermal stress. Geomorphology 41, 23–35.
Hall, K., André, M.F., 2003. Rock thermal data at the grain scale: Applicability to granular disintegration in cold environments. Earth Surface Processes and Landforms 28, 823–836.
Hall, K., André, M.-F., 2006. Temperature observations in Antarctic tafoni: Implications for weathering, biological colonization, and tafoni formation. Antarctic Science 18, 377–384.

Hall, R.D., Michaud, D., 1988. The use of hornblende etching, clast weathering and soils to date alpine glacial and periglacial deposits: A study from southwestern Montana. Geological Society of America Bulletin 100, 458–467.
Hall, K., Otte, W., 1990. A note on biological weathering on nunataks of the Juneau Icefield, Alaska. Permafrost and Periglacial Processes 1, 189–196.
Hall, K., Thorn, C., 2011. The historical legacy of spatial scales in cold region weathering: Misrepresentation and resulting misdirection. Geomorphology 130, 83–90.
Hall, K., Thorn, C.E., Sumner, A., 2012. On the persistence of 'weathering'. Geomorphology 149-150, 1–10.
Hellmann, R., Wirth, R., Daval, D., Barnes, J.P., Penisson, J.M., Tisserand, D., Epicier, T., Florin, B., Hervig, R.L., 2012. Unifying natural and laboratory chemical weathering with interfacial dissolution–reprecipitation: A study based on the nanometer-scale chemistry of fluid–silicate interfaces. Chemical Geology 294, 203–216.
Hiebert, F.K., Bennett, P.C., 1992. Microbial control of silicate weathering in organic-rich ground water. Science 258, 278–281.
Hobbs, W.H., 1919. Earth features and their meaning. In: An introduction to geology for the student and the general reader. MacMillan, New York.
Hobbs, D.W., 1967. The formation of tension joints in sedimentary rocks: An explanation. Geological Magazine 104, 550–556.
Hochella, M.F., 2002a. Nanoscience and technology: The next revolution in the Earth sciences. Earth and Planetary Science Letters 203, 593–605.
Hochella, M.F., 2002b. There's plenty of room at the bottom: Nanoscience in geochemistry. Geochimica Cosmochimica Acta 66, 735–743.
Hochella, M.F., Banfield, J.F., 1995. Chemical weathering of silicates in nature: A microscopic perspective with theoretical considerations. In: White, A.F., Brantley, S.L. (Eds.), Chemical weathering rates of silicate minerals. Mineralogical Society of America, Washington D.C, pp. 353–406.
Hochella, M.F., Lower, S.K., Maurice, P.A., Penn, R.L., Sahai, N., Sparks, D.L., Twining, B.S., 2008. Nanominerals, mineral nanoparticles, and earth systems. Science 319, 1631–1635.
Holmes, A., 1965. Principles of physical geology. Ronald Press, New York, 1288 p.
Hovelmann, J., Putnis, C.V., Benning, L.G., 2018. Metal sequestration through coupled dissolution– precipitation at the brucite–water interface. Minerals 8. https://doi.org/10.3390/min8080346.
Howard, A.D., 1994. A detachment-limited model of drainage basin evolution. Water Resources Research 30, 2261–2285.
Israel, E.J., Arvidson, R.E., Wang, A., Pasteris, J.D., Jolliff, B.L., 1997. Laser Raman spectroscopy of varnished basalt and implications for in situ measurements of Martian rocks. Journal of Geophysical Research-Planets 102 (E12), 28705–28716.
Jeong, A., Lee, J.I., Seong, Y.B., Balco, G., Yoo, K.-C., Yoon, H.I., Domack, E., Rhee, H.H., Yu, B.Y., 2018. Late Quaternary deglacial history across the Larsen B embayment, Antartica. Quaternary Science Reviews 189, 134–148.
Johnson, J.R., Christensen, P.R., Lucey, P.G., 2002. Dust coatings on basaltic rocks and implications for thermal infrared spectroscopy of Mars. Journal of Geophysical Research-Planets 107 (E6). Art No. 5035.
Jordan, D.W., 1954. The adhesion of dust particles. British Journal of Applied Physics 5, S194–S198.
Kalinichev, A.G., Wang, J., Kirkpatrick, R.J., 2007. Molecular dynamics modeling of the structure, dynamics and energetics of mineral-water interfaces: Applications to cement materials. Cement and Concrete Research 37, 337–347.
Kleber, A., 1997. Cover-beds as soil parent materials in midlatitude regions. Catena 30, 197–213.
Koning, D.J., Mansell, M., 2017. Rockfall susceptibility maps for New Mexico. In: New Mexico Bureau of Geology and Mineral Resources Open-file Report 595, pp. 1–41.
Koopal, L.K., Goloub, T., de Keizer, A., Sidorova, M.P., 1999. The effect of cationic surfactants on wetting, colloid stability and flotation of silica. Colloids and Surfaces A: Physicochemical and Engineering Aspects 151, 15–25.
Korschinek, G., Bergmaier, A., Faestermann, T., Gerstmann, U.C., Knie, K., Rugel, G., Wallner, A., Dillmann, I., Dollinger, G., von Gostomski, C.L., Kossert, K., Maiti, M., Poutivtsev, M., Remmert, A., 2010. A new value for the half-life of 10Be by Heavy-Ion Elastic Recoil Detection and liquid scintillation counting. Nuclear Instruments and Methods in Physics Research Section B Beam Interactions With Material and Atoms 268, 187–191.
Kraft, M.D., Michalski, J.R., Sharp, T.G., 2004. High-silica rock coatings: TES surface-type 2 and chemical weathering on Mars. Lunar and Planetary Science 35, 1936.pdf.
Krinsley, D., 1998. Models of rock varnish formation constrained by high resolution transmission electron microscopy. Sedimentology 45, 711–725.
Krinsley, D., Dorn, R.I., Anderson, S., 1990. Factors that may interfere with the dating of rock varnish. Physical Geography 11, 97–119.
Krinsley, D.H., Dorn, R.I., Tovey, N.K., 1995. Nanometer-scale layering in rock varnish: Implications for genesis and paleoenvironmental interpretation. Journal of Geology 103, 106–113.
Krinsley, D., Dorn, R.I., DiGregorio, B.E., 2009. Astrobiological implications of rock varnish in Tibet. Astrobiology 9, 551–562.
Krinsley, D.H., Dorn, R.I., DiGregorio, B.E., Razink, J., Fisher, R., 2017. Mn-Fe enhancing budding bacteria in century-old rock varnish, Erie Canal, New York. Journal of Geology 125, 317–336.
Kumar, R., Jefferson, I.F., O'Hara-Dhand, K., Smalley, I.J., 2006. Controls on quartz silt formation by crystalline defects. Naturwissenschaften 93, 185–188.
Langworthy, K., Krinsley, D., Dorn, R.I., 2010. High resolution transmission electron microscopy evaluation of silica glaze reveals new textures. Earth Surface Processes and Landforms 35, 1615–1620.
Larson, P.H., Dorn, R.I., 2014. Strath development in small-arid watersheds: Case study of South Mountain, Sonoran Desert, Arizona. American Journal of Science 314, 1202–1223.
Larson, P.H., Dorn, R.I., Palmer, R.E., Bowles, Z., Harrison, E., Kelley, S., Schmeeckle, M.W., Douglass, J., 2014. Pediment response to drainage basin evolution in south-central Arizona. Physical Geography 35, 369–389.
Larson, P.H., Kelley, S.B., Dorn, R.I., Seong, Y.B., 2016. Pace of landscape change and pediment development in the northeastern Sonoran Desert, United States. Annals of the Association of American Geographers 106, 1195–1216.
Lebatard, A.-E., Bourlès, D.L., Braucher, R., Arnold, M., Duringer, P., Jolivet, M., Moussa, A., Deschamps, P., Roquin, C., Carcaillet, J., Schuster, M., Lihoreau, F., Likius, A., Mackaye, H.T., Vignaud, P., Brunet, M., 2010. Application of the authigenic 10Be/9Be dating method to continental sediments: Reconstruction of the Mio-Pleistocene sedimentary sequence in the early hominid fossiliferous areas of the northern Chad Basin. Earth and Planetary Science Letters 297, 57–70.
Lee, M.R., 2010. Transmission electron microscopy (TEM) of Earth and planetary materials: A review. Mineralogical Magazine 74, 1–27.
Lee, M.R., Parsons, I., 1995. Microtextural controls of weathering of perthitic alkali feldspars. Geochimica et Cosmochimica Acta 59, 4465–4488.
Lee, M.R., Brown, D.J., Smith, C.L., Hodson, M.E., Mackenzie, M., Hellman, R., 2007. Characterization of mineral surfaces using FIB and TEM: A case study of naturally-weathered alkali feldspars. American Mineralogist 92, 1383–1394.
Li, Z., Liu, L., Chen, J., Teng, H.H., 2016. Cellular dissolution at hypha-and spore-mineral interfaces revealing unrecognized mechanisms and scales of fungal weathering. Geology 44, 319–322.
Liu, T., 2003. Blind testing of rock varnish microstratigraphy as a chronometric indicator: Results on late Quaternary lava flows in the Mojave Desert, California. Geomorphology 53, 209–234.
Liu, T., 2010. VML dating lab. http://www.vmldating.com/ last accessed 1 October 2010.
Liu, T., Broecker, W.S., 2000. How fast does rock varnish grow? Geology 28, 183–186.
Liu, T., Broecker, W.S., 2007. Holocene rock varnish microstratigraphy and its chronometric application in drylands of western USA. Geomorphology 84, 1–21.
Liu, T., Broecker, W.S., 2008a. Rock varnish evidence for latest Pleistocene millennial-scale wet events in the drylands of western United States. Geology 36, 403–406.
Liu, T., Broecker, W.S., 2008b. Rock varnish microlamination dating of late Quaternary geomorphic features in the drylands of the western USA. Geomorphology 93, 501–523.
Liu, T., Broecker, W.S., Bell, J.W., Mandeville, C., 2000. Terminal Pleistocene wet event recorded in rock varnish from the Las Vegas Valley, southern Nevada. Palaeogeography, Palaeoclimatology, Palaeoecology 161, 423–433.
Locke, W.W., 1979. Etching of hornblende grains in arctic soils: An indicator of relative age and paleoclimate. Quaternary Research 11, 197–212.

Locke, W.W., 1986. Rates of hornblende etching in soils on glacial deposits, Baffin Island, Canada. Academic Press, New York, pp. 129–145.
Lower, S.K., Hochella, M.F., Beveridge, T.J., 2001. Bacterial recognition of mineral surfaces: Nanoscale interactions between Shewanella and alpha-FeOOH. Science 292, 1360–1363.
Lybrand, R.A., Austin, J.C., Fedenko, J., Gallery, R.E., Rooney, E., Schroeder, P.A., Zaharescu, D.G., Qafoku, O., 2019. A coupled microscopy approach to assess the nano-landscape of weathering. Scientific Reports 9, 5377. https://doi.org/10.1038/s41598-019-41357-0.
Macholdt, D.S., Jochum, K.P., Pöhlker, C., Stoll, B., Weis, U., Weber, B., Muller, M., Kappl, M., Buhre, S., Kilcoyne, A.L.D., Weigand, M., Scholtz, D., Al-Amri, A.M., Andreae, M.O., 2015. Microanalytical methods for in-situ high-resolution analysis of rock varnish at the micrometer to nanometer scale. Chemical Geology 411, 57–68.
Mantha, H., Schindler, M., Hochella, M.F., 2019. Occurrence and formation of incidental metallic Cu and CuS nanoparticles in organic-rich contaminated surface soils in Timmins, Ontario. Environmental Science: Nano. https://doi.org/10.1039/C8EN00994E.
Masarik, J., Beer, J., 2009. An updated simulation of particle fluxes and cosmogenic nuclide production in the Earth's atmosphere. Journal of Geophysical Research 114, D11103. https://doi.org/10.1029/2008JD010557.
Matsuoka, N., Oguchi, C.T., Fukushi, K., Matsushi, Y., Yokoyama, T., 2017a. Overview of the special issue "rock weathering from nanoscale to global scale: 1. Microscopic weathering and basic studies". Journal of Geography (Chigaku Zasshi) 126, 263–265.
Matsuoka, N., Waragai, T., Wakasa, S.A., 2017b. Linking laboratory experiments, field observations, and natural features. Journal of Geography (Chigaku Zasshi) 126, 369–405.
McAlister, J.J., Smith, B.J., Torok, A., 2006. Element partitioning and potential mobility within surface dusts on buildings in a polluted urban environment, Budapest. Atmospheric Environment 40, 6780–6790.
McKeown, D.A., Post, J.E., 2001. Characterization of manganese oxide mineralogy in rock varnish and dendrites using X-ray absorption spectroscopy. American Mineralogist 86, 701–713.
McKnight, T.L., 1993. Physical geography: A landscape appreciation. Prentice-Hall, Englewood Cliffs, New Jersey.
Meek, N., Douglass, J., 2001. Lake overflow: An alternative hypothesis for Grand Canyon incision and development of the Colorado River. In: Young, R.A., Spamer, E.E. (Eds.), Colorado river: Origin and evolution. Grand Canyon Association, Grand Canyon, Arizona, pp. 199–204.
Merrill, G.P., 1906. A treatise on rocks, rock-weathering, and soils. Macmillan, New York, 400 p.
Meunier, A., Sardini, P., Robinet, J.C., Pret, D., 2007. The petrography of weathering processes: Facts and outlooks. Clay Minerals 42, 415–435.
Mitchell, R.L., Davies, P., Kenrick, P., Volkenandt, T., Pleydell-Pearce, C., Johnston, R., 2021. Correlative microscopy: A tool for understanding soil weathering in modern analogues of early terrestrial biospheres. Scientific Reports 11, 1–14. https://doi.org/10.1038/s41598-021-92184-1.
Mol, L., Viles, H., 2012. The role of rock surface hardness and internal moisture in tafoni development in sandstone. Earth Surface Processes and Landforms 37, 301–314.
Molnar, P., Anderson, R.S., Andersson, S.P., 2007. Tectonics, fracturing of rock, and erosion. Journal of Geophysical Research Earth Surface 112. https://doi.org/10.1029/2005JF000433.
Moss, A.J., Green, P., 1998. Sand and silt graints: Predetermination of their formation and properties by microfractures in quartz. Australian Journal of Earth Sciences 22, 485–495.
Mottershead, D.N., Pye, K., 1994. Tafoni on coastal slopes, South Devon, U.K. Earth Surface Processes and Landforms 19, 543–563.
Navarre-Sitchler, A., Brantley, S., 2007. Basalt weathering across scales. Earth and Planetary Science Letters 261, 321–334.
Nishiyama, N., Yokoyama, T., 2017. Distribution of water in Rock: From outcrop scale to nanometer scale. Journal of Geography (Chigaku Zasshi) 126, 311–323.
Ollier, C.D., 1965. Dirt cracking—A type of insolation weathering. Australian Journal of Science 27, 236–237.
Paradise, T.R., 1995. Sandstone weathering thresholds in Petra, Jordan. Physical Geography 16, 205–222.
Paradise, T.R., 2013. Tafoni and other rock basins. In: Pope, G.A. (Ed.), Treatise on geomorphology, Weathering and soils geomorphology, vol. 4. Academic Press, San Diego, pp. 111–126.
Pearthree, P.A., House, P.K., 2014. Paleogeomorphology and evolution of the early Colorado River inferred from relationships in Mohave and Cottonwood valleys, Arizona, California, and Nevada. Geosphere 10, 1139–1160.
Péwé, T.L., 1978. Guidebook to the Geology of Central Arizona. In: Arizona Bureau of Geology and Mineral Technology Special Paper 2.
Phillips, J.D., 2000. Signatures of divergence and self-organization in soils and weathering profiles. Journal of Geology 108, 91–102.
Pope, G.A., 1995. Newly discovered submicron-scale weathering in quartz: Geographical implications. Professional Geographer 47, 375–387.
Pope, G.A., 2015. Regolith and weathering (rock decay) in the critical zone. Developments in Earth Surface Processes 19, 113–145.
Pope, G., Dorn, R.I., Dixon, J., 1995. A new conceptual model for understanding geographical variations in weathering. Annals of the Association of American Geographers 85, 38–64.
Pope, G.A., Meierding, T.C., Paradise, T.R., 2002. Geomorphology's role in the study of weathering of cultural stone. Geomorphology 47, 211–225.
Potter, R.M., 1979. The tetravalent manganese oxides: Clarification of their structural variations and relationships and characterization of their occurrence in the terrestrial weathering environment as desert varnish and other manganese oxides. Ph.D. Dissertation [Ph.D. Dissertation thesis]. California Institute of Technology, Pasadena.
Potter, R.M., Rossman, G.R., 1977. Desert varnish: The importance of clay minerals. Science 196, 1446–1448.
Putnis, C.V., 2019. Editoral for special issue "mineral surface reactions at the nanoscale". Minerals 9. https://doi.org/10.3390/min9030185.
Putnis, C.V., Ruiz-Agudo, E., 2013. The mineral-water interface: Where minerals react with the environment. Elements 9, 177–182.
Pye, K., 1987. Aeolian dust and dust deposits. Academic Press, London.
Pye, K., 1989. Processes of fine particle formation, dust source regions, and climatic change. Kluwer Academic Publishers, Dordrecht, pp. 3–30.
Rapp, A., 1960. Recent development of mountain slopes in Karkevagge and surroundings, Northern Scandinavia. Geografiska Annaler 42A, 71–201.
Reith, F., 2011. Life in the deep subsurface. Geology 39, 287–288.
Robinson, D.A., Williams, R.B.G., 1992. Sandstone weathering in the High Atlas, Morocco. Zeitschrift fur Geomorphologie 36, 413–429.
Scheidegger, A.E., 2001. Surface joint systems, tectonic stresses and geomorphology: A reconciliation of conflicting observations. Geomorphology 38, 213–219.
Schiffbauer, J.D., Xiao, S., 2009. Novel application of focused ion beam electron microscopy (FIB-EM) in preparation and analysis of microfossil ultrastructures: A new view of complexity in early eukaryotic organisms. Palaios 24, 616–626.
Schmeeckle, T., Smith, N., Convey, D., Fewell, J.H., Dorn, R.I., 2021. Experimental evidence of ants' role in the carbon cycle: Ant extracts rapidly increase biological weathering under laboratory conditions.
Schultz, R.A., 2000. Growth of geologic fractures into large-strain populations: Review of nomenclature, subcritical crack growth, and some implications for rock engineering. International Journal of Rock Mechanics and Mining Sciences 37, 403–411.
Schwartzman, D.W., 2002. Life, temperature and the Earth. Columbia University Press, New Yock, 272 p.
Schwartzman, D.W., 2017. Life's critical role in the long-term carbon cycle: The biotic enhancement of weathering. AIMS Geosciences 3, 216–238.
Schwartzman, D.W., Volk, T., 1989. Biotic enhancement of weathering and the habitability of Earth. Nature 340, 457–460.
Scott, D.N., Wohl, E.E., 2018. Bedrock fracture influences on geomorphic process and form across process domains and scales. Earth Surface Processes and Landforms 1–19. https://doi.org/10.1002/esp.4473.
Seong, Y.B., Jeong, A., Dorn, R.I., Gootee, B.F., House, P.K., Pearthree, P.A., 2016. Age of bouse formation estimated by authenic 10Be/9Be dating. In: GSA Annual Meeting. Denver, CO. https://doi.org/10.1130/abs/2016AM-284185.
Seong, Y.B., Dorn, R.I., Yu, B.Y., 2016a. Evaluating the life expectancy of a desert pavement. Earth-Science Reviews 162, 129–154.
Seong, Y.B., Larson, P.H., Dorn, R.I., Yu, B.Y., 2016b. Evaluating process domains in small granitic watersheds: Case study of Pima Wash, South Mountains, Sonoran Desert, USA. Geomorphology 255, 108–124.

Sharma, R.K., Gupta, H.O., 1993. Dust pollution at the Taj Mahal—A case study. In: Thiel, M.-J. (Ed.), Conservation of stone and other materials. E & FN Spon, London, pp. 11–18.
Shtober-Zisu, N., Brook, A., Kopel, D., Roberts, D., Ichoku, C., Wittenberg, L., 2018. Fire induced rock spalls as long-term traps for ash. Catena 162, 88–99.
Smalley, I.J., Krinsley, D.H., 1978. Loess deposits associated with deserts. Catena 5, 53–66.
Smalley, I.J., Kumar, R., Dhand, K.O., Jefferson, I.F., Evans, R.D., 2005. The formation of silt material for terrestrial sediments: Particularly loess and dust. Sedimentary Geology 179, 321–328.
Smith, R.J., Horgan, B.H.N., 2021. Nanoscale variations in natural amorphous and nanocrystalline weathering products in mafic to intermediate volcanic terrains on Earth: Implications for amorphous detections on Mars. Journal of Geophysical Research Planets, e2020JE006769. https://doi.org/10.1029/2020JE006769.
Smith, B.J., McAlister, J.J., Baptista-Neto, J.A., Silva, M.A.M., 2007. Post-depositional modification of atmospheric dust on a granite building in central Rio de Janeiro: implications for surface induration and subsequent stone decay. Geological Society, London, Special Publications 271, 153–166.
Smits, M.M., Herrmann, A.M., Duane, M., Duckworth, O.W., Bonneville, S., Benning, L.G., Lundstrom, U., 2009. The fungal–mineral interface: Challenges and considerations of micro-analytical developments. Fungal Biology Review 23, 122–131.
Song, W., Ogawa, N., Oguichi, C.T., Hatta, T., Matsukura, Y., 2010. Laboratory experiments on bacterial weathering of granite and its constituent minerals. Géomorphologie, Relief, Processus, Environnement 5, 327–336.
St Clair, J., Moon, S., Holbrook, W.S., Perron, J.T., Riebe, C.S., Martel, S.J., Carr, B., Harman, C., Singha, K., deB Richter, D., 2015. Geophysical imaging reveals topographic stress control of bedrock weathering. Science 350, 534–538.
Stoppato, M.C., Bini, A., 2003. Deserts. Firely Books, Buffalo, 256 p.
Šujan, M., Braucher, R., Kováč, M., Bourlès, D.L., Rybár, S., Guillou, V., Hudáčková, N., 2016. Application of the authigenic 10Be/9Be dating method to Late Miocene–Pliocene sequences in the northern Danube Basin (Pannonian Basin System): Confirmation of heterochronous evolution of sedimentary environments. Global and Planetary Change 137, 35–53.
Swoboda-Colberg, N.G., Drever, J.I., 1993. Mineral dissolution rates in plot-scale field and laboratory experiments. Chemical Geology 105, 51–69.
Tang, R., Wang, L., Orme, C.A., Bonstein, T., Bush, P.J., Nancollas, G.H., 2004. Dissolution at the nanoscale: Self-preservation of biominerals. Angewandte Chemie 43, 2697–2701.
Thoma, S.G., Gallegos, D.P., Smith, D.M., 1992. Impact of fracture coatings on fracture/matrix flow interactions in unsaturated, porous media. Water Resources Research 28, 1357–1367.
Thorn, C.E., Dixon, J.C., Darmody, R.G., Rissing, J.M., 1989. Weathering trends in fine debris beneath a snow patch, Niwot Ridge, Front Range, Colorado. Physical Geography 10, 307–321.
Thorn, C.E., Darmody, R.G., Dixon, J.C., Schlyter, P., 2001. The chemical weathering regime of Karkevagge, arctic-alpine Sweden. Geomorphology 41, 37–52.
Thorn, C.E., Dixon, J.C., Darmody, R.G., Allan, C.E., 2006. Ten years (1994-2004) of "potential" weathering in Kärkevagge , Swedish Lapland. Catena 65, 272–278.
Tratebas, A.M., Cerveny, N., Dorn, R.I., 2004. The effects of fire on rock art: Microscopic evidence reveals the importance of weathering rinds. Physical Geography 25, 313–333.
Turkington, A.V., Paradise, T.R., 2005. Sandstone weathering: A century of research and innovation. Geomorphology 67, 229–253.
Turkington, A.V., Phillips, J.D., Campbell, S.W., 2005. Weathering and landscape evolution. Geomorphology 67, 1–6.
Twidale, C.R., 2002. The two-stage concept of landform and landscape development involving etching: Origin, development and implications of an idea. Earth Science Reviews 57, 37–74.
Twidale, C.R., Bourne, J.A., 1978. Bornhardts. Zeitschrift fur Geomorphology Supplementband 31, 111–137.
Van Vliet-Lanoë, B., Fox, C.A., 2018. Frost action. In: Stoops, G., Marcelino, V., Mees, F. (Eds.), Interpretation of micromorphological features of soils and regoliths. Elsevier, Amsterdam, pp. 575–603.
Velbel, M.A., 1993. Constancy of silicate-mineral weathering-rate ratios between natural and experimental weathering: Implications for hydrologic control of differences in absolute rates. Chemical Geology 105, 89–99.
Viles, H.A., 2001. Scale issues in weathering studies. Geomorphology 41, 61–72.
Villa, N., Dorn, R.I., Clark, J., 1995. Fine material in rock fractures: Aeolian dust or weathering? In: Tchakerian, V. (Ed.), Desert aeolian processes. Chapman & Hall, London, pp. 219–231.
von Blanckenburg, F., Bouchez, J., Wittman, H., 2012. Earth surface erosion and weathering from the ^{10}Be (meteoric)/^{9}Be ratio. Earth and Planetary Science Letters 351, 295–305.
Wadsten, T., Moberg, R., 1985. Calcium oxalate hydrates on the surface of lichens. Lichenologist 17, 239–245.
Walder, J.S., Hallet, B., 1986. The physical basis of frost weathering: Toward a more fundamental and unified perspective. Arctic and Alpine Research 18, 27–32.
Wang, J.Z., Kalinichev, A.G., Kirkpatrick, R.J., 2006. Effects of substrate structure and composition on the structure, dynamics, and energetics of water at mineral surfaces: A molecular dynamics modeling study. Geochimica Cosmochimica Acta 70, 562–582.
Washburn, A.L., 1969. Case hardening. In: Washburn, A.L. (Ed.), Weathering, frost action and patterned ground in the mesters district. Northeast Greenland, Reitzels, Copenhagen, p. 15.
Wasklewicz, T., 1994. Importance of environment on the order of mineral weathering in olivine basalts, Hawaii. Earth Surface Processes and Landforms 19, 715–735.
Wasklewicz, T., Dorn, R.I., Clark, S., Hetrick, J., Pope, G., Liu, T., Krinsley, D.H., Dixon, J., Moore, R.B., Clark, J., 1993. Olivine does not necessarily weather first. Journal of Tropical Geography 14, 72–80.
Waychunas, G.A., Kim, C.S., Banfield, J.F., 2005. Nanoparticle iron oxide minerals in soils and sediments: Unique properties and contaminant scavenging mechanisms. Journal of Nanoparticle Research 7, 409–433.
Wei, H., Sparks, R.S.J., Liu, R., Fan, Q., Wang, Y., Hong, H., Zhang, H., Chen, H., Jiang, C., Dong, J., Zheng, Y., Pan, Y., 2003. Three active volcanoes in China and their hazards. Journal of Asian Earth Sciences 21, 515–526.
Whalley, W.B., Marshall, J.R., Smith, B.J., 1982. Origin of desert loess from some experimental observations. Nature 300, 433–435.
White, A.F., 2005. Natural weathering rates of silicate minerals. Elsevier, Amsterdam, pp. 133–168.
White, D.A., Fink, D., Post, A.L., Simon, K., Galton-Fenzi, B., Foster, S., Fujioka, T., Jeromson, M.R., Blaxell, M., Yokoyama, Y., 2019. Beryllium isotope signatures of ice shelves and sub-ice shelf circulation. Earth and Planetary Science Letters 505, 86–95.
Wild, B., Imfeld, G., Daval, D., 2021. Direct Measurement of fungal contribution to silicate weathering rates in soil. Geology 49. https://doi.org/10.1130/G48706.1.
Wilhelmy, H., 1964. Cavernous rock surfaces in semi-arid and arid climates. Pakistan Geographical Review 19 (2), 8–13.
Willenbring, J.K., von Blanckenburg, F., 2010. Meteoric cosmogenic Beryllium-10 adsorbed to river sediment and soil: Applications for Earth-surface dynamics. Earth-Science Reviews 98, 105–122.
Wright, J., Smith, B., Whalley, W.B., 1998. Mechanisms of loess-sized quartz silt production and their relative effectiveness: Laboratory simulations. Geomophology 23, 15–34.
Xu, K., Cao, P., Heath, J.R., 2010. Graphene visualizes the first water adlayers on mica at ambient conditions. Science 329, 1188–1191.
Yaalon, D.H., Ganor, E., 1973. The influence of dust on the soils during the Quaternary. Soil Science 116, 146–155.
Yokoyama, T., Nishiyama, N., 2017. Reactive transport processes from outcrop scale to nano scale. Journal of Geography (Chigaku Zasshi) 126, 297–310.
Yokoyama, Y., Anderson, J.B., Yamane, M., Simkins, L.M., Miyairi, Y., Yamazaki, T., Koizumi, M., Suga, H., Kusahara, K., Prothro, L., Hasumi, H., Southon, J.R., Ohkouchi, N., 2016. Widespread collapse of the Ross Ice Shelf during the late Holocene. Proceedings of the National Academy of Sciences of the United States of America 113, 2354 LP – 2359.
You, C.-F., Lee, T., Li, Y.-H., 1989. The partition of Be between soil and water. Chemical Geology 77, 105–118.
Young, R.W., 1988. Quartz etching and sandstone karst: Examles from the East Kimberleys, Northwestern Australia. Zeitschrift fur Geomorphologie 32, 409–423.
Young, R., Young, A.R.M., 1992. Sandstone landforms. Springer-Verlag, Berlin.

Zhang, H., Gilbert, B., Huang, F., Banfield, J.F., 2003. Water-driven structure transformation in nanoparticles at room temperature. Nature 424, 1025–1029.
Zhou, B.G., Liu, T., Zhang, Y.M., 2000. Rock varnish microlaminations from northern Tianshan, Xinjiang and their paleoclimatic implications. Chinese Science Bulletin 45, 372–376.
Zhu, C., Veblen, D.R., Blum, A.E., Chipera, S.J., 2006. Naturally weathered feldspar surfaces in the Navajo Sandstone aquifer, Black Mesa, Arizona: Electron microscopic characterization. Geochimica Cosmochimica Acta 70, 4600–4616.
Zorin, Z.M., Churaev, N., Esipova, N., Sergeeva, I., Sobolev, V., Gasanov, E., 1992. Influence of cationic surfactant on the surface charge of silica and on the stability of acqueous wetting films. Journal of Colloid and Interface Science 152, 170–182.
Zou, Z., Habraken, W.J., Matveeva, G., Jensen, A.C., Bertinetti, L., Hood, M.A., Sun, C.Y., Gilbert, P.U., Polishchuk, I., Pokroy, B., Mahamid, J., 2019. A hydrated crystalline calcium carbonate phase: Calcium carbonate hemihydrate. Science 363 (6), 396–400.